The Remote Sensing of Marine Plastics

Zane William Havens
Albion, MI

Bachelor of Arts, Albion College, 2012

A Thesis presented to the Graduate Faculty

of the University of Virginia in Candidacy for the Degree of Master of Arts

Department of Environmental Sciences

University of Virginia

May, 2018

ABSTRACT

Marine debris pollution is one of the most ubiquitous and pressing environmental issues affecting our oceans today. Increased demand for new polymer products alongside the longevity and resistance to decomposition of the plastics currently in existence offers ocean ecosystems little relief from the barrage of mismanaged plastic waste that enters waters globally. Clean up efforts have been implemented across the planet with the goal of combating this scourge; however, resources to accomplish this goal are limited and the afflicted area is vast. With the assistance of remote sensing, mitigation efforts can be applied tactfully to maximize positive impacts while limiting expenditure of resources. Remotely sensed data can be applied indirectly, providing parameters for models predicting the paths of marine debris throughout the world's oceans, or directly, using remote sensors to locate areas with concentrations of debris in need of remediation. Although remote sensing technology has yet to achieve the resolution and accuracy to be relied on solely in this application, it has the potential to be a very useful tool in the fight to rid oceans of marine debris.

TABLE OF CONTENTS

ABSTRACT i
LIST OF FIGURES iii
LIST OF TABLES v
LIST OF EQUATIONS v
LIST OF ABBREVIATIONS vi
ACKNOWLEDGEMENTS viii
1. Introduction 1
    1.1 Plastics in Marine Ecosystems 3
    1.2 Plastic Micro-litter and Nano-litter 5
    1.3 Detriment to Human Health 6
    1.4 The Role of Remote Sensing in Regards to Marine Debris 7
2. Remote Sensing Used in Models 10
    2.1 SCUD 11
    2.2 OSCAR 11
    2.3 SURCOUF 12
    2.4 CTOH Surface Current Data Product 13
    2.5 Potential for OGCM Improvement 18
3. VIS Remote Sensing of Marine Debris 19
    3.1 Coastal Webcams 20
    3.2 Balloon Photography 20
    3.3 Small Aircraft Photography 21
    3.4 VIS Satellite Imagery 24
4. Hyperspectral Remote Sensing of Marine Debris 24
    4.1 Terrestrial Remote Sensing of Plastics 24
    4.2 Hyperspectral Remote Sensing in a Marine Environment 26
    4.3 Modeling Plastic Reflectance 27
    4.4 Laboratory Based Hyperspectral Sensing 29
    4.5 Vibrational Microspectroscopy 30
    4.6 Aerial and Satellite Hyperspectral Detection 32
5. SAR Detection of Marine Debris 37
6. Application of Marine Debris Detection Data 39
7. Conclusion 42
8. References 43

LIST OF FIGURES

Figure 1. Historic and predicted cumulative plastic waste generation and disposal, 1950 to 2050. Solid lines represent historic data, while dashed lines represent predictions (Geyer *et al*., 2017). 2

Figure 2. Reported number of entanglements/ingestion by taxonomic group. Charts show total number of individuals (a.), total number of species (b.), and total papers involving marine debris entanglement/ingestion (SCBD, 2012). 3

Figure 3. Reported incidents of marine debris entanglement/ingestion by decade (SCBD, 2012). 4

Figure 4. Testing of impact resistance of 3 plastic materials after being subjected to a period of outdoor weathering (Summers & Rabinovitch, 1999). 6

Figure 5. Example of SCUD model output (Maximenko & Hafner, 2010). Modeled surface current velocities for August 20, 2008. Current velocities are in cm/s. 12

Figure 6. Monthly composite for OSCAR model runs during December 1996 (Lagerloef *et al*., 1999). Top chart shows Ekman velocities, middle chart shows Geostrophic velocities, and the bottom chart shows the sum of the Ekman and Geostrophic velocities. Data for these plots were subsampled to a 1° X 5° grid. 15

Figure 7. SURCOUF model output for the Indian Ocean (Larnicol *et al*., 2006). Top represents cumulative currents for July-August, 2005 and bottom shows cumulative surface currents for January-February, 2006. 16

Figure 8. Standard deviation for the CTOH model from 2000-2006 (Sudre & Morrow, 2008). Standard deviation is shown to be lower at high latitude and subtropical regions. 17

Figure 9. Sample imagery pulled from mosaic image taken from an aircraft over the Hawaiian Islands (Moy *et al*., 2018). Red boxes indicate items identified as debris in this image. Yellow boxes exhibit other types of debris not included in this particular image. 23

Figure 10. Normalized reflectance spectra of 12 plastic materials (Vázquez-Guardado *et al*., 2015) 25

Figure 11. Reflectance spectra of unknown marine-harvested plastics. Shaded regions indicate common absorption features (Garaba & Dierssen, 2018). 35

Figure 12. Comparison of reflectance spectra of wet and dry micro-plastics. Shaded regions indicate common spectral absorption features (Garaba & Dierssen, 2018). 36

Figure 13. Hydrocarbon index map of Sunshine Canyon Landfill (Garaba & Dierssen, 2018). Left image shows the index for absorption feature at 1732, right image shows index for absorption feature 1215 nm. Higher index value indicates higher likelihood of hydrocarbon material. 36

Figure 14. Aerial photos (top) of tsunami debris and PALSAR images (bottom) taken on March 13th (left) and March 19th, 2011 (Arii *et al*., 2014). Colored shapes denote classification of debris. 39

Figure 15. Proposed Ocean Cleanup Passive Collector (Slat, 2014). Image shows extended barriers in orange funneling plastics towards the collection platform. 41

LIST OF TABLES

Table 1. Reproductive health effects in adult males associated with phthalate concentrations (Meeker et al., 2009). Phthalates include di(2-ethylhexyl) phthalate (DEHP), dibutyl phthalate (DBP), mono-ethyl phthalate (MEP), mono-(2-ethylhexyl) phthalate (MEHP), mono-butyl phthalate (MBP), and mono-benzyl phthalate (MBzP). 8

Table 2. Pre-natal health outcomes in relation to concentration of phthalates (Meeker et al., 2009). Phthalates include mono-(2-ethyl-5-oxohexyl) phthalate (MEOHP), mono-(2-ethyl-5-hydroxylhexyl) phthalate (MEHHP), MEHP, MEP, and MBP. 8

Table 3. Models and the remotely sensed information used as parameters. 14

Table 4. List of variables for Equation 1, used to compute fraction of plastic surface coverage (Goddijn-Murphy et al., 2018).....28

Table 5. Confusion matrix showing actual class vs. predicted class in terms of pixel percentage classified as polyethylene (PE), polypropylene (PP), and polystyrene (PS) (Serranti et al., 2018). 30

Table 6. Comparison between Raman imaging and FTIR transmission imaging when used to detect marine micro-plastics (Kappler et al., 2016).....31

Table 7. Specifications of SAR sensors used to identify tsunami debris (Arii, Koiwa, & Aoki, 2014). 37

LIST OF EQUATIONS

Equation 1. Equation for determining fractional plastic coverage per pixel (Goddijn-Murphy *et al.*, 2018).....28

Equation 2. Equation determining recommended SAR swath width (X), using maximum observed velocity of debris Vmax and time interval (T) (Arii, Koiwa, & Aoki, 2014). 39

LIST OF ABBREVIATIONS

ABS	Acrylonitrile butadiene styrene
AOML	Atlantic Oceanographic and Meteorological Laboratory
AVIRIS	Airborne Visible / Infrared Imaging Spectrometer
AVISO	Archiving, Validation and Interpretation of Satellite Oceanographic
AVHRR	Advanced Very High –Resolution Radiometer
CLS	Collecte Localisation Satellites
CTOH	the Centre de Topographie des Océans et de l'Hydrosphère
DBP	Dibutyl phthalate
DEHP	Di(2-ethylhexyl) phthalate
DMSP	Meteorological Satellite Program
EMR	Electromagnetic Radiation
FTIR	Fourier-transform infrared spectroscopy
GRACE	Gravity Recovery and Climate Experiment satellite
MBP	Mono-butyl phthalate
MBzP	Mono-benzyl phthalate
MDOT	Mean dynamic ocean topography
MDP	Marine Debris Pollution
MEHHP	Mono-(2-ethyl-5-hydroxylhexyl) phthalate
MEHP	Mono-(2-ethylhexyl) phthalate
MEOHP	Mono-(2-ethyl-5-oxohexyl) phthalate
MEP	Mono-ethyl phthalate
MIR	Mid-wavelength infrared radiation, 3000-8000 nm
MSLA	Mapped sea level anomaly
MT	Metric tons
NIR	Near-infrared radiation, 750-1400 nm

NOAA	National Oceanic and Atmospheric Administration
OGCM	Ocean General Circulation Model
OSCAR	Ocean Surface Current Analysis Real-time
POP	Persistent organic pollutant
PVC	Polyvinyl chloride
QuikSCAT	Quik Scatterometer
SAR	synthetic aperture radar
SCBD	Secretariat of the Convention of Biological Diversity
SCUD	Surface CUrrents from Diagnostic model
SSM/I	Special Sensor Microwave Imager
SURCOUF	Surface Currents Field
SWIR	Short-wavelength infrared radiation, 1400-3000 nm
UV	Ultraviolet spectrum, 10-390 nm
VIS	Visible spectrum, 390-700 nm

ACKNOWLEDGMENTS

I would like to thank my advisor, Stephen Macko, for his guidance while I pursued my Master's Degree and his valuable feedback on this thesis.

I would like to thank my thesis committee members, Xi Yang, John Porter, and Sunnie Capelle, for their willingness to review my work and the time they devoted to ensuring I succeed.

I would like to thank Sonia Foley who, despite having her own academic quagmire to trudge through, has been there to support me and keep me sane during this past year.

I would like to thank my parents, Keith and Susan Havens, for their undying support of my goal and their sage advice.

Finally, I would like to thank everyone involved in the Environmental Sciences Department at the University of Virginia, both the faculty and the students, for all they do to make being a part of this department a wonderful experience.

1. Introduction

The very earliest known polymer can be dated to Mesoamerica, 1600 BC; this rubber-like substance was processed from a latex drawn from the *Castilla elastica* tree and liquid extracted from the Morning Glory Vine *Ipomoea alba*, and was used to make figurines, bands and balls used in games (Hosler, 1999). Other early polymers were made of natural materials such sap from trees and cellulose from wood fiber and were mostly used in jewelry for the upper class. It was not until the invention of vulcanized rubber in the 1830's that this class of materials became more accessible to the general population, but these products were still limited by the scarcity of the natural resources required to manufacture the useful substance (Wiebe *et al.,* 1987). The invention of the easily molded and durable plastic-like material Parkesine by Alexander Parkes in 1855 aimed to combat this by utilizing more common natural materials, but it was not until 1907 that the first fully synthetic plastic, Bakelite, was invented (Gloag, 1943). This discovery allowed for the rapid production of material that had no need for natural resources like wood or rubber. This substance, branded as "the material of 1000 uses", led the world into the 20th century on a wave of cheap, durable, and easily molded polymers.

Today, plastics are ubiquitous in society. With the multitude of uses, it is no wonder that the production of plastic products has had an 8.6% compound annual growth rate since the 1950s (PlasticsEurope, 2016). However, continuous use of these durable, non-deteriorative substances has led to an ever-increasing build-up of plastic waste (Andrady & Neal, 2009; Barnes *et al.,* 1985). Geyer *et al.* (2017) predict that, by

2050, 12 billion metric tons (MT) of plastic will have been deposited in landfills or the natural environment (Figure 1). Much of this plastic finds its way to ocean environments; Jambeck *et al.* (2016) estimates that in 2010, approximately 2.5 billion MT of municipal waste was generated by people living in coastal countries and, on average, 68% of this waste was mismanaged (mismanaged being defined by Jambeck *et al.* as either littered or inadequately disposed).

According to Andrady (2003), plastic pollution can be categorized into four general categories: mega-litter, macro-litter, meso-litter, and micro-litter. Mega-litter can be identified as being over 15 cm in diameter; this can include anything from enormous floating docks to plastic shopping bags. Macro-litter ranges from 10 mm - 15 cm and includes plastic items easily identified by eye. Ranging in size from 5 - 10 mm, meso-litter consists of deteriorated plastics and virgin resin pellets. Finally, micro-litter

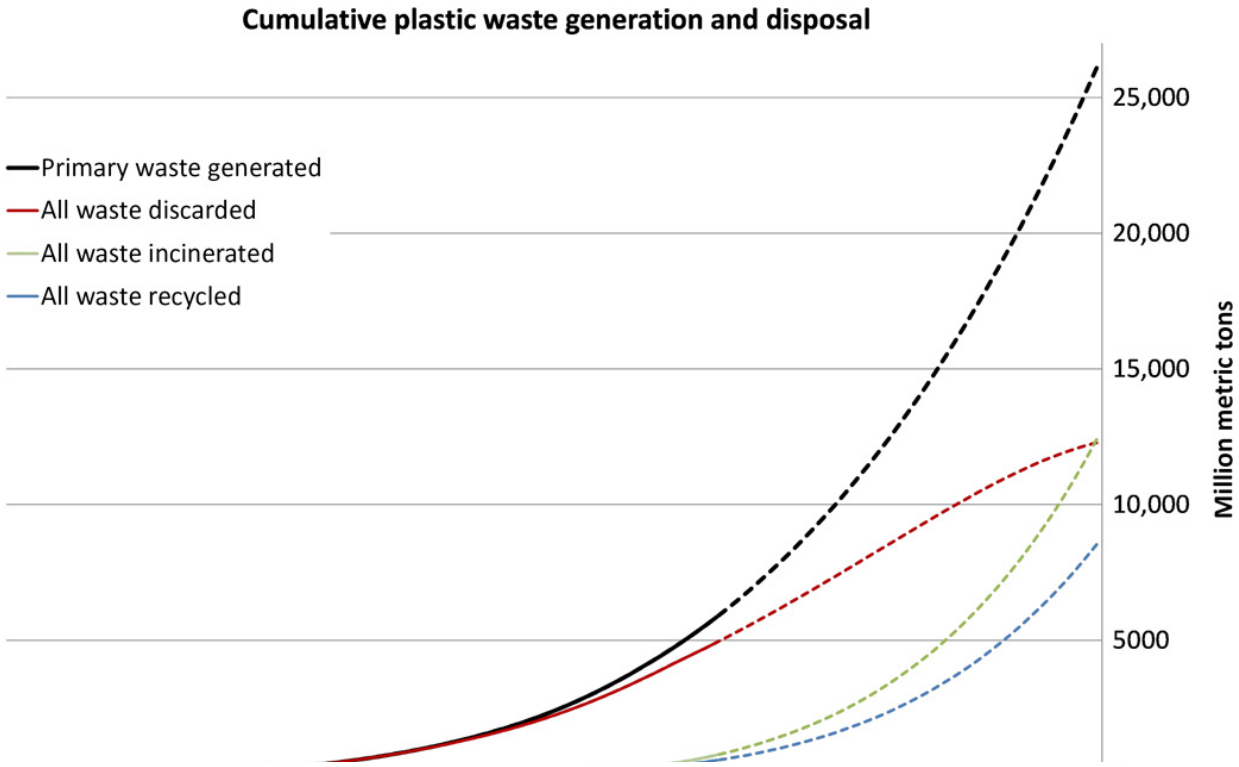

Figure 1. Historic and predicted cumulative plastic waste generation and disposal, 1950 to 2050. Solid lines represent historic data, while dashed lines represent predictions (Geyer et al., 2017).

encompasses anything less than 5 mm in diameter. Within this micro-litter category, Mattsson *et al*. (2015) define another category, nano-plastics. These particles have at least two dimensions between 1 and 100 nm.

1.1 Plastics in Marine Ecosystems

In 2010, it was estimated that 12.7 million MT of plastics entered the ocean from 127 coastal countries (Jambeck *et al*, 2015). These plastics accumulate and cause harm to marine life by causing entanglement, inhibiting movement (NOAA, 2014a) and by being ingested and causing digestive blockage (NOAA, 2014b). In 2012, the

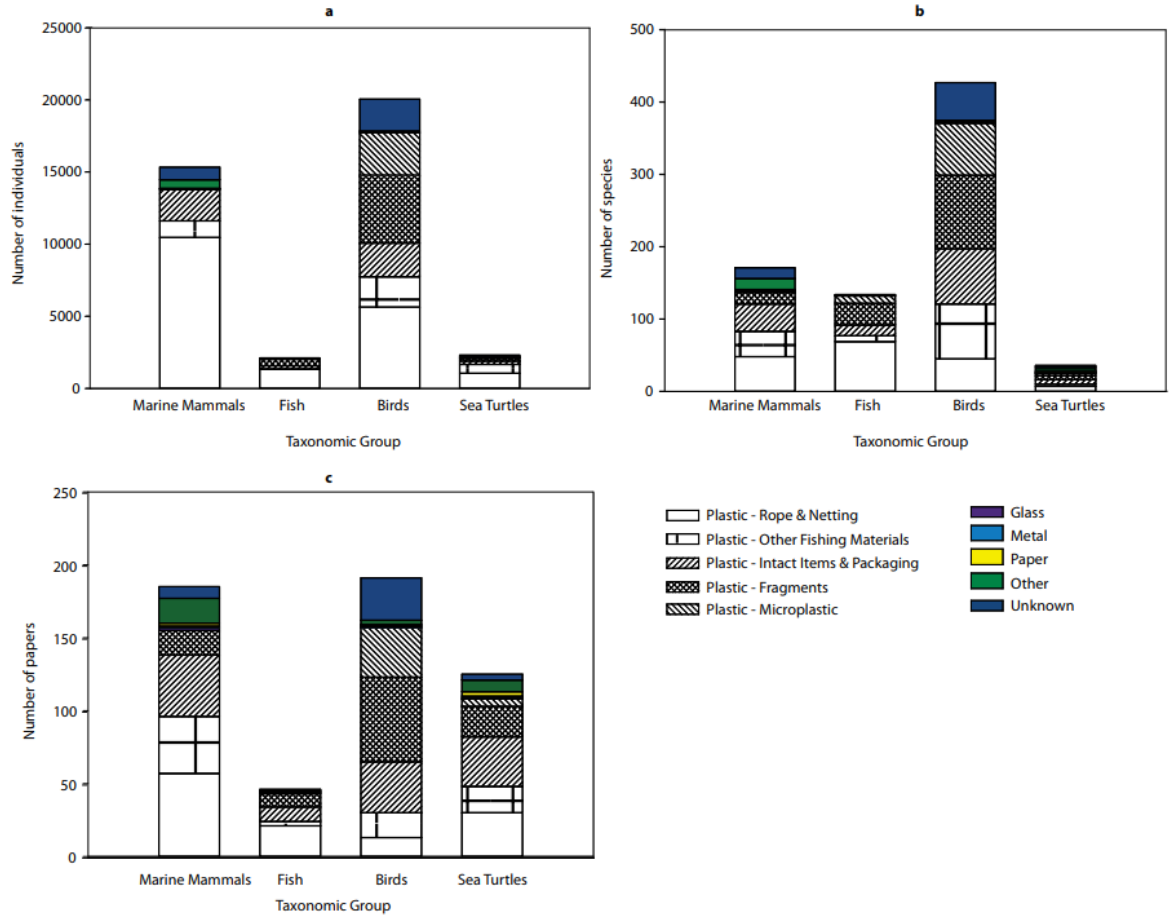

Figure 2. Reported number of entanglements/ingestion by taxonomic group. Charts show total number of individuals (a.), total number of species (b.), and total papers involving marine debris entanglement/ingestion (SCBD, 2012).

Secretariat of the Convention on Biological Diversity (SCBD) found the majority of reported marine debris pollution (MDP) entanglement and ingestion cases were caused by plastic debris (Figure 2). The SCBD found that the number of reported entanglement/ingestion cases has increased since the 1960s, suggesting that this problem is occurring more frequently (Figure 3).

With the transport of floating plastics comes an often-overlooked potential issue: transport and introduction of invasive species (NOAA, 2015). Biofilms of algae, bacteria, and cyanobacteria can colonize floating debris and thrive in the marine environment. Bio-foulers including barnacles, mussels, and macroalgae can attach to surfaces of large debris and travel thousands of kilometers. Even terrestrial organisms can be transported via larger rafts of debris. Although there are currently no reported cases of introduction of invasive species via MDP (NOAA, 2015), MDP as a pathway for species invasion is a potential challenge that should not be ignored.

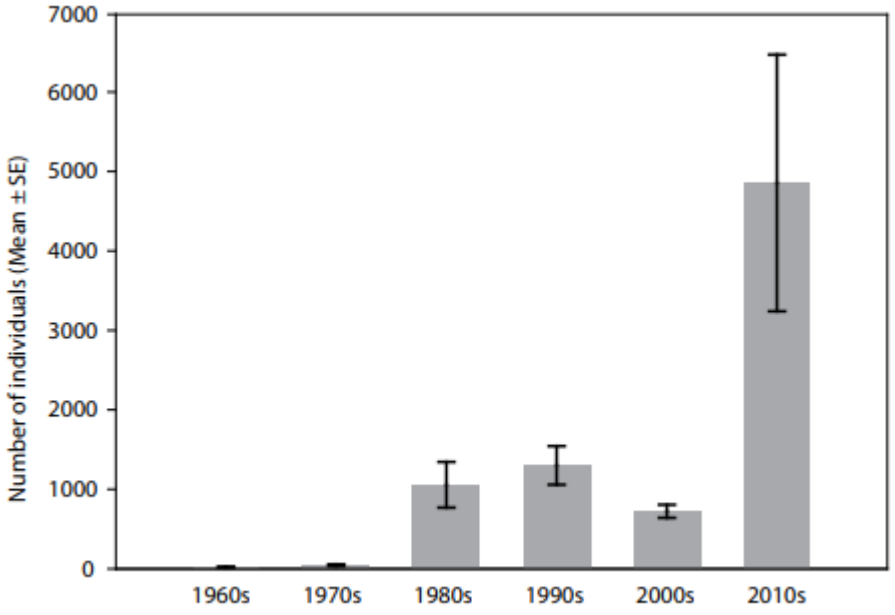

Figure 3. Reported incidents of marine debris entanglement/ingestion by decade (SCBD, 2012).

1.2 Plastic Microlitter and Nanolitter

Plastic micro-litter can either be made intentionally (“microbeads” used in facial scrubs and cosmetics (Cheung & Fok, 2017) or virgin plastic resin pellets), or come from the deterioration of larger plastic objects (Cooper & Corcoran, 2010). As these plastic compounds are exposed to the elements, disintegration begins, and the plastics break apart to form even smaller particles. These smaller micro-plastics can become ingested by filter feeding organisms that are unable to differentiate between plastic and plankton (Moore *et al*., 2001). Nano and micro-plastics have been found in every ocean, including waters rarely traversed by humans (Cincinelli *et al.,* 2017).

This disintegration of plastics is largely an effect of radiation in the visible spectrum (VIS) and ultraviolet spectrum (UV). The energy from this radiation is absorbed by plastics and breaks the chemical bonds; combined with other factors such as temperature, moisture, and oxidation, this photodegradation process weakens the plastic, allowing for its weathering (Andrady, 2003). This chemical process, combined with other chemical and physical processes associated with a marine environment, has the potential to weather plastics to nano-litter, where they can enter cells via endocytosis (Andrady, 2011; Mattsson *et al.,* 2015). This phenomena comes with another set of environmental problems, as plastics have the propensity to absorb persistent organic pollutants (POPs), hazardous chemicals that can be harmful to ocean wildlife. With nano-plastics laden with POPs entering the marine trophic system at its most basic level, the entire ecosystem is at risk (Auta *et al.,* 2017).

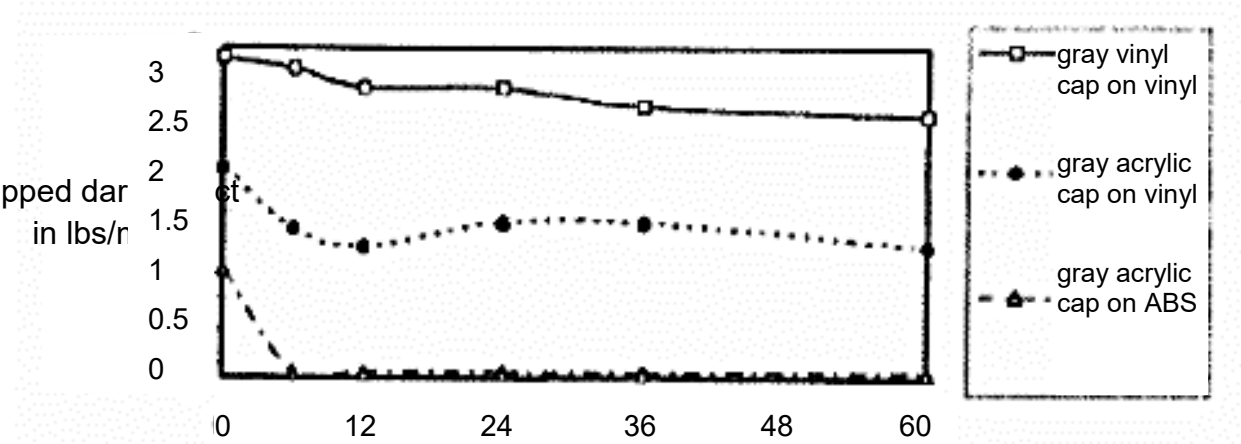

Figure 4. Testing of impact resistance of 3 plastic materials after being subjected to a period of outdoor weathering (Summers & Rabinovitch, 1999).

The time that plastics take to disintegrate varies based on the type of plastic and the chemical stabilizers added to the resins to reinforce the plastic. For example, Summers and Rabinovitch (1999) tested the impact resistance of polyvinyl chloride (PVC) and acrylonitrile butadiene styrene (ABS) when subjected to the outdoor weathering environments of Ohio and Arizona and found that ABS drastically lost impact resistance after just 5 months in both climates, while PVC retained impact resistance past 2 years (Figure 4). Considering that the removal of micro-plastics from the marine environment is virtually impossible and that there is a significant period of time before larger plastic items weather to micro-plastics, it is imperative that point sources of plastic pollution be identified immediately and that the removal of meso-litter and macro-litter from the oceans should be accomplished efficiently and with great haste.

1.3 Detriment to Human Health

The effects of plastic pollution on human health is a field that is not entirely understood (Thompson *et al.,* 2009). Aside from the obvious effects of entanglement with plastic debris while swimming in waters tainted with plastic pollution, one of the

major concerns related to plastic pollution is the exposure to toxic chemical additives found in many plastics. Bisphenol A (BPA) and phthalates are among the chemicals used as additives in plastics, and these chemicals are thought to be endocrine disrupting compounds. Several studies focusing on these particular chemicals suggest a relationship between the presence of these plastic additives in urine and decreased sperm quality in men (Table 1) (Meeker *et al.*, 2009). Additionally, studies (Table 2) have suggested that there is a link between the presence of these compounds in a mother's urine and the genital development of her unborn child (Meeker *et al.*, 2009).

One of the paths through which these chemicals can enter the body is through ingestion; considering the increasing presence of nano-plastics in natural waters, the likelihood that these chemicals will be ingested by humans via the consumption of seafood laden with nano-plastics will be greater as MDP continues.

1.4 The Role of Remote Sensing in Regards to Marine Debris

MDP is a global issue; studies have shown that debris can travel thousands of kilometers in a matter of months (Maes and Blanke, 2015; Duhec *et al.*, 2015). In order to effectively remedy a global environmental calamity such as MDP pollution, it is imperative to utilize methods that can cheaply and efficiently observe large areas with high frequency. Remote sensing technology shows the potential to achieve this goal.

The applications for remote sensing in this field are varied. Sensors can be utilized in a lab or mounted on land, drones, aircraft, and satellites, and can measure data throughout the electromagnetic radiation (EMR) spectrum (Campbell and Wynne, 2011). These measurements can span in observable area from micrometers to meters to kilometers, and the information collected can be used to directly identify MDP or used

Table 1. Reproductive health effects in adult males associated with phthalate concentrations (Meeker et al., 2009). Phthalates include di(2-ethylhexyl) phthalate (DEHP), dibutyl phthalate (DBP), mono-ethyl phthalate (MEP), mono-(2-ethylhexyl) phthalate (MEHP), mono-butyl phthalate (MBP), and mono-benzyl phthalate (MBzP).

Phthalate or metabolite (measured in urine unless otherwise noted)	Outcome
MEP, MEHP	Increased sperm DNA damage
MEP	Increased sperm DNA damage
MBP	Decreased sperm motility
MBP, MBzP	Decreased sperm concentration
DBP and DEHP in semen samples	Decreased sperm motility
MBP	Decreased free testosterone, increased lutenizing hormone/free testosterone
MBzP	Decreased follicle stimulating hormone
MEP	Decreased sperm motility, reduced lutenizing hormone

Table 2. Pre-natal health outcomes in relation to concentration of phthalates (Meeker et al., 2009). Phthalates include mono-(2-ethyl-5-oxohexyl) phthalate (MEOHP), mono-(2-ethyl-5-hydroxylhexyl) phthalate (MEHHP), MEHP, MEP, and MBP.

Phthalate or metabolite (measured in urine unless otherwise noted)	Outcome
MEHP (in cord blood)	Shorter gestational age at birth
MEHP, MEOHP, MEHHP, MEP, MBP	Shorter anogenital distance (in males)
MEHP	Reduced penile size (in males)
MEHP, MEHHP, MEOHP	Incomplete testicular descent (in males)

indirectly as real-time parameters for models (NOAA, 2016b).

Although MDP as it is defined by the National Oceanic and Atmospheric Administration (NOAA) can include all sorts of litter, ranging from rubber tires to wooden docks, focusing on plastic litter for the purposes of remote sensing is advisable bearing in mind plastics' relative abundance as a marine pollutant and its tendency to persist in marine environments (NOAA, 2016a). Assuming that plastics comprise the majority of MDP simplifies detection methods and behavioral predictions.

Of the properties of plastic litter to be considered in its remote identification, one stands above all: plastics often float. This characteristic is both helpful and harmful in the mission to rid marine environments of plastic; it allows for easier detection of the debris from an aerial perspective, but also allows for the debris to change location with ocean currents. Although MDP can be found virtually anywhere in our oceans, there are several gyres throughout our oceans where much of this floating debris accumulates. Currently, 5 gyres have been recognized as the major collectors of MDP: The North Atlantic Gyre, the South Atlantic Gyre, the Indian Ocean Gyre, the North Pacific Gyre, and the South Pacific Gyre (NOAA, 2016b). These gyres are located in the center of circular currents systems resulting from Ekman (Coriolis Effect driven) flows and contain higher concentrations of floating MDP due to the deflection of water towards the center of the gyre by these currents. There are several models forecasting geostrophic (pressure gradient driven) and Ekman currents using historical measurements of salinity, temperature, depth, and wind direction. However, these models are more accurate for retrospective analysis and tend to work best on short temporal scales, normally less than 72 hours (NOAA, 2016b).

Remote sensing techniques offer a wide range of applications in regards to identifying and locating MDP. Although the current state of remote sensing technology may not be advanced enough to be relied upon exclusively when detecting and tracking MDP, when used as a supplemental source of data, remote sensing has the potential to change the way sources and sinks of MDP are ascertained and to aid remediation efforts across our oceans. The intention of this study is to assess the progress that has been made in the field of MDP remote sensing while evaluating the role this technology might play in future efforts to detect and remove MDP.

2. Remote Sensing used in Models

One application of remote sensing in the field of MDP mitigation comes from the need for accurate model inputs to determine ocean surface currents. Using Ocean General Circulation Models (OGCM), predictions can be made about the paths of MDP, and this information can assist in identifying sources of MDP and locations where MDP might accumulate. Although many OGCMs do not require remotely sensed data to predict ocean currents (Ingraham, 1997; Zelenke *et al*., 2012), those that do require measurements that can range from wind speed and direction to mapped sea level anomaly (MSLA) that are virtually impossible to measure *in situ* on a global scale. These components are used to calculate both geostrophic and Ekman currents, allowing for the user to predict changes in the currents on a scale of days to weeks, depending on the spatial resolution required. To fine tune the model, geographic and current information from floating buoys are used. Although this method of determining the paths and velocity of debris does not involve directly detecting the debris, the data from remotely sensed sources can play a major role in increasing the accuracy of these

models and helps predict the ocean surface currents that carry MDP over longer durations (Dohan & Maximenko, 2010) (Table 3).

2.1 SCUD

As an example, the Surface CUrrents from Diagnostic model (SCUD), an OGCM developed by NOAA, is used to predict current velocities on a global scale and utilizes horizontal pressure gradients and surface wind velocity and direction derived from satellite data (Figure 5) (Maximenko & Hafner, 2010). To determine geostrophic current components, remotely sensed MSLA data is taken from the Archiving, Validation and Interpretation of Satellite Oceanographic (AVISO) satellite altimetry data server, which is comprised of measurements collected from all altimeter satellites available at the time of measurement, alongside mean dynamic ocean topography (MDOT) data, derived using altimetry and gravitational anomaly data collected from the Gravity Recovery and Climate Experiment satellite (GRACE). To calculate Ekman currents, wind velocity and direction data are collected using measurements from the Quik Scatterometer (QuikSCAT) satellite. QuikSCAT uses microwave pulses emitted from orbiting scatterometers to calculate sea surface roughness, which is then used as a proxy for wind velocity (Jet Propulsion Laboratory, 2001). Finally, SCUD uses the GPS coordinates of drifter buoys to fine tune model predictions (Maximenko & Hafner, 2010).

2.2 OSCAR

The California Institute of Technology's Ocean Surface Current Analysis Real-time (OSCAR) is another model that uses remotely collected data to model ocean currents (Figure 6). To determine geostrophic currents, MSLA data is obtained from the

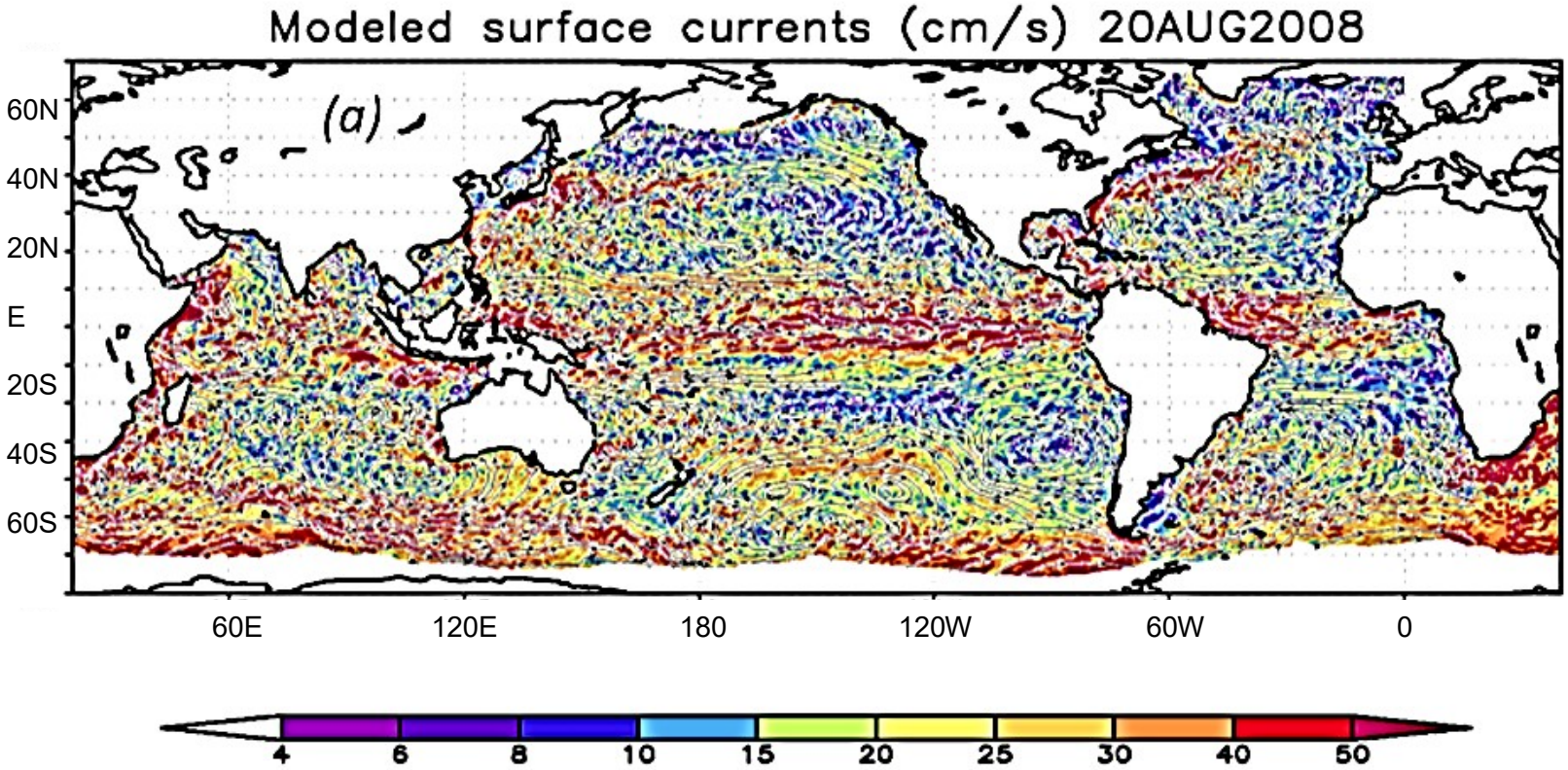

Figure 5. Example of SCUD model output (Maximenko & Hafner, 2010). Modeled surface current velocities for August 20, 2008. Current velocities are in cm/s.

TOPEX/Poseidon satellite, an instrument equipped with a sensor that uses a technique referred to as “precise orbit determination” to establish an exact height of the sensor, combined with a measurement of distance between the satellite and the ocean surface calculated by sending microwave pulses to the ocean surface and recording the time it takes to return to the satellite (Jet Propulsion Laboratory, n.d.). This method provides MSLA an accuracy of 3 cm.

Wind data is determined using the Special Sensor Microwave Imager (SSM/I), carried aboard Defense Meteorological Satellite Program (DMSP) satellites. This information is calculated in a similar manner to the QuikSCAT data used by SCUD, utilizing microwave emissivity brightness associated with sea surface roughness as a proxy for wind vector components (Hong and Shin, 2012). This, alongside the sea surface altimetry data collected from TOPEX/Poseidon and sea surface temperature data collected from the Advanced Very High-Resolution Radiometer (AVHRR) imager carried aboard the NOAA-15 satellite (“NOAA Satellite Information System (NOAASIS),” 2017), is used to calculate wind surface layer velocity, which is used in turn to calculate Ekman currents. The OSCAR model works best when used to predict large scale (>= 5° longitude) and low frequency (>= 20 day) variations in surface flow (Bonjean & Lagerloef, 2002; Lagerloef *et al.,* 1999).

2.3 SURCOUF

Developed by the French Operation Oceanography Mercator-Ocean project and the Collecte Localisation Satellites (CLS), the Surface Currents Field (SURCOUF) OGCM also uses MSLA (collected via Jason1 and ENVISAT sensors), wind stress (collected via QuikSCAT), and MDPOT data (collected via GOCE) to calculate

geostrophic currents and Ekman currents. According to Larnicol *et al*., (2006), this model produced an error less than 40% (when compared to measurements from buoy velocities from the Atlantic Oceanographic and Meteorological Laboratory (AOML) database) in the zonal direction, with higher errors in the meridional direction. Figure 7 shows an example of the SURCOUF model output for the Indian Ocean in 2006.

2.4 CTOH Surface Current Data Product

Another OGCM that produces surface current prediction with the assistance of remotely sensed parameters, the Centre de Topographie des Océans et de l'Hydrosphère (CTOH) surface current data product model predicts geostrophic currents using MSLA calculated from altimetry data from 5 altimeter missions (TOPEX/Poseidon, ERS1&2, Geosat Follow-on, Envisat, and Jason-1) and MDPOT data obtained from

Table 3. Models and the remotely sensed information used as parameters.

Model	Organization	Data Collected	Satellite
SCUD	NOAA	MSLA	several, AVISO data server
		Wind direction/velocity	QuikSCAT
		MDPOT	GRACE
OSCAR	California Institute of Technology	MSLA	TOPEX/Poseidon
		Wind direction/velocity	SSM/I (DMSP)
		Sea surface temperature	AVHRR
SURCOUF	CLS	MSLA	SL-TAC
		MDPOT	GOCE
CTOH surface current data product	CTOH	MSLA	TOPEX/Poseidon, ERS1&2, Geosat Follow-on, Envisat, Jason-1
		Wind direction/velocity	QuikSCAT
		MDPOT	GRACE

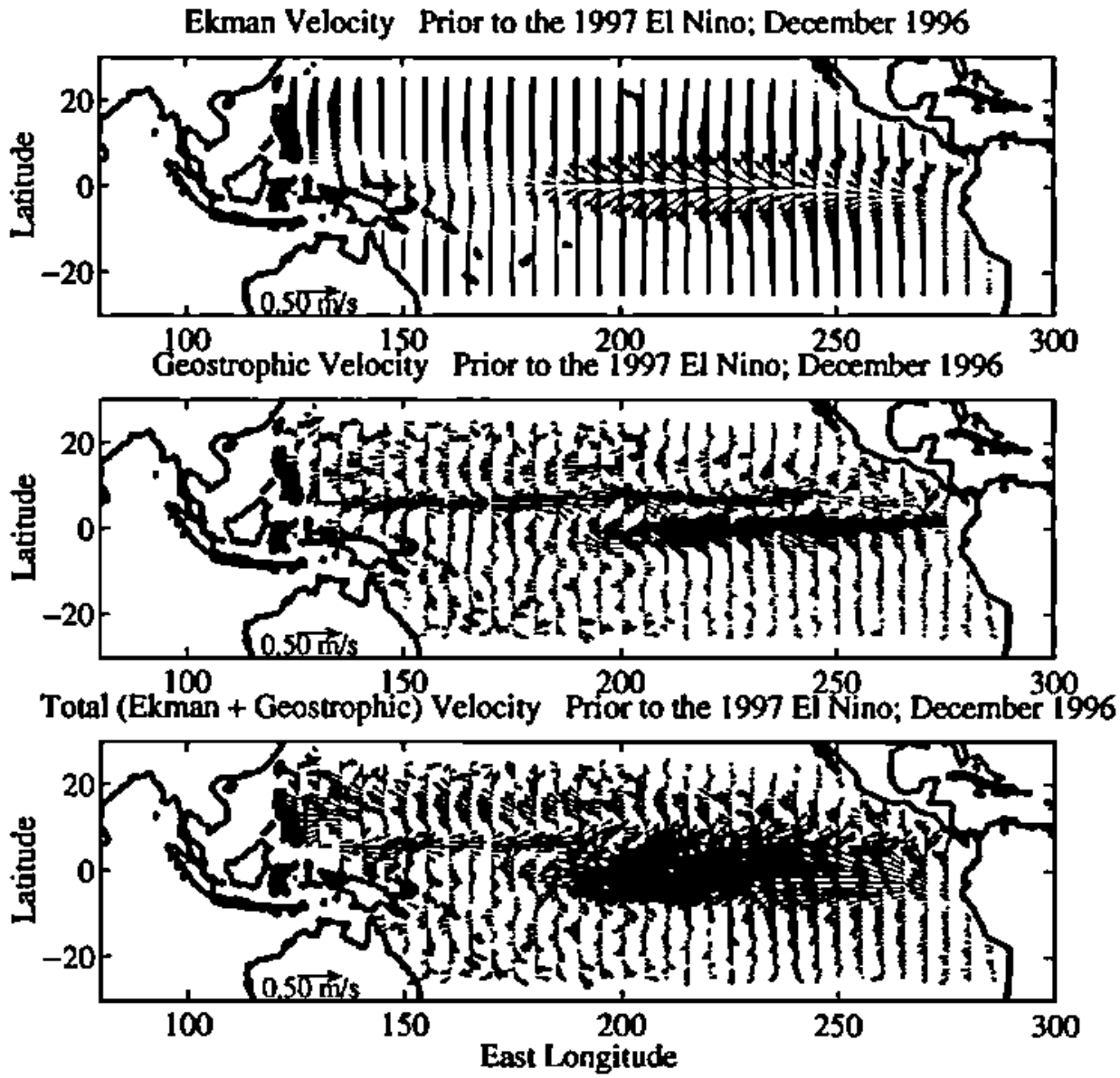

Figure 6. Monthly composite for OSCAR model runs during December 1996 (Lagerloef et al., 1999). Top chart shows Ekman velocities, middle chart shows Geostrophic velocities, and the bottom chart shows the sum of the Ekman and Geostrophic velocities. Data for these plots were subsampled to a 1° X 5° grid.

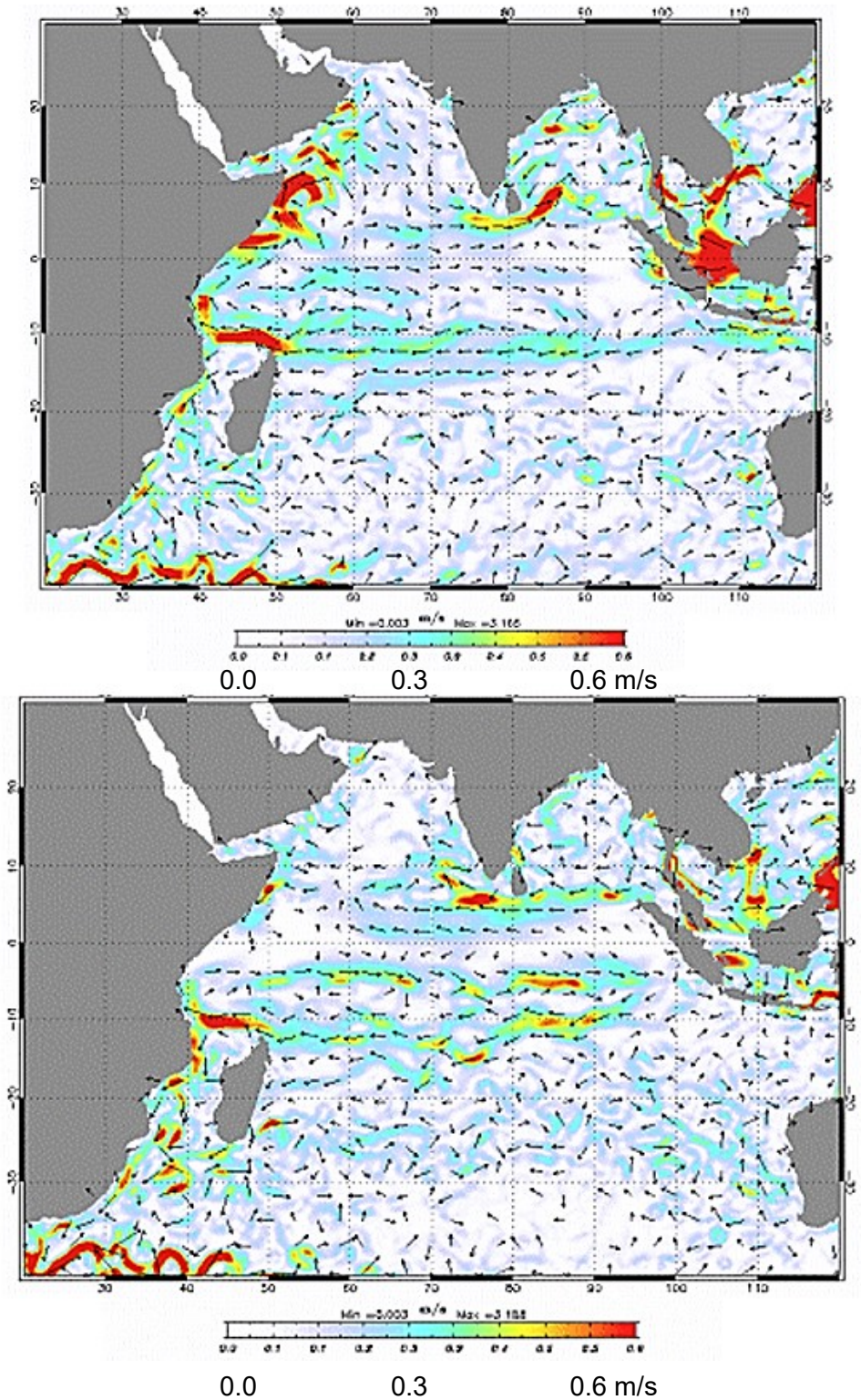

Figure 7. SURCOUF model output for the Indian Ocean (Larnicol et al., 2006). Top represents cumulative currents for July-August, 2005 and bottom shows cumulative surface currents for January-February, 2006.

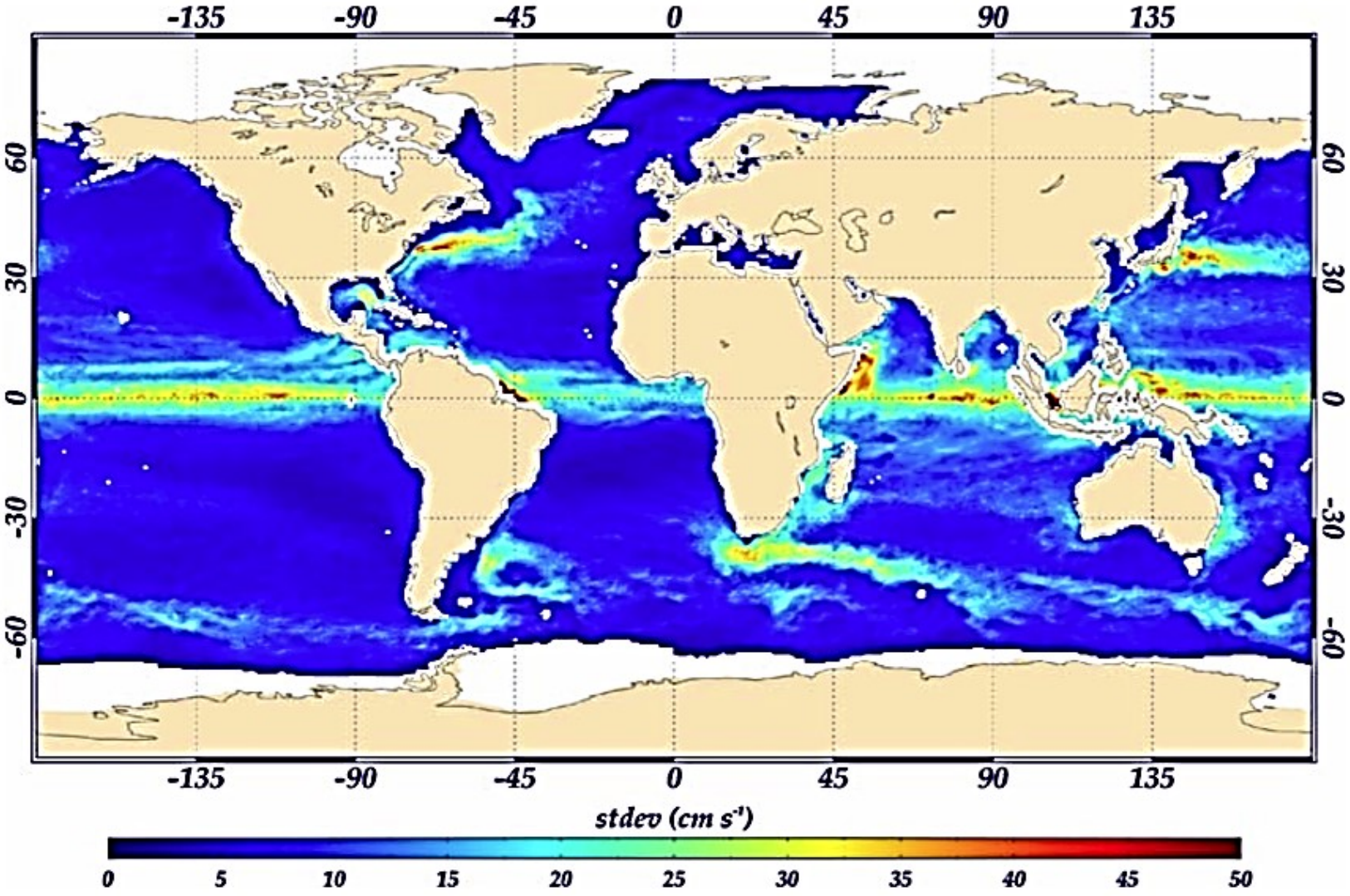

Figure 8. Standard deviation for the CTOH model from 2000-2006 (Sudre & Morrow, 2008). Standard deviation is shown to be lower at high latitude and subtropical regions.

GRACE. To determine Ekman currents, wind stress components were determined using information pulled from QuikSCAT. This model showed relatively strong correlations with drifter buoy data in the subtropical to high latitude bands with r values between 0.7-0.9 (Sudre & Morrow, 2008) (Figure 8).

2.5 Potential for OGCM Improvement

With the increasing resolution of remote sensors, models that utilize remotely sensed data are becoming more accurate and are able to model surface currents at even finer resolutions (0.1° or less). However, these models are nowhere near perfect, and there is certainly room for improvement in distinct areas. Dohan and Maximenko (2010) identify 5 areas where these models could use development:

- The majority of plastic pollution originates on land (Jambeck *et al.,* 2015), but OGCMs struggle to accurately represent currents within 25 km of the shoreline. This is partially due to the addition of certain variables, such as tidal signals and seafloor shape, which increase the frequency of current shifts. Additionally, altimeter data, a component that is crucial in each of the above models, is unreliable near land as a result of atmospheric effects and modulation in the altimeter waveform.
- Modeling small scale features has become possible with increased resolution in remotely sensed data, but this is an area where OGCMs can see improvement. In recent years, increased resolution and blended satellite products have allowed scientists to detect mesoscale eddies; between the mesoscale eddies are smaller eddies that are distorted into a filamentous shape by the presence of these larger mesoscale eddies. Even with the

increased resolution of current data, these features are difficult to detect using satellite data, and are not always included in current models.

- The majority of satellite measurements used in OGCMs focus on ocean surface properties; models that draw parameters from this data make assumptions about the vertical structure of these currents that are not necessarily true. Dohan and Maximenko propose that a vertical shear component to these models could account for changes in water density that affect the transport of suspended objects, such as MDP.
- When Ekman currents are predicted using OGCMs, mean wind velocities are calculated and assumed to be steady. However, in reality winds are anything but consistent. Dohan and Maximenko suggest that a component that accounts for relatively sudden changes in wind direction and velocity, such as storm systems, is needed to accurately represent Ekman spirals, and this cannot be considered with the diurnal measurements provide by the current sensors.
- Dohan and Maximenko argue that to fully understand ocean current circulation, information on the behavior of the subsurface is required. Currently, there is some data on ocean currents at depth from profiling floats with the ability to sink to depths of 2000 m. Considering the difficulties associated with monitoring subsurface variables of thermohaline circulation remotely, these devices have proven to be very useful in expanding our understanding of ocean processes.

3. VIS Remote Sensing of Marine Debris

A common method of directly remote sensing MDP uses the VIS spectrum of EMR, from approximately 390 nm to 700 nm. Sensors that can be used to track and identify MDP using this spectrum range from coastal cameras to cameras mounted on low flying aircraft to satellite-based sensors (Nakashima *et al*., 2011; Kako *et al*., 2012; Moy *et al*., 2018). These sensors have varying spatial and temporal resolutions and scales, owing to the variety of vehicles used to carry the remote sensing devices.

3.1 Coastal Webcams

While coastal cameras can capture nearshore debris and debris deposited on shorelines, they lack the ability to track the marine movements of debris on a global scale. In 2010, Kako *et al.* studied marine litter deposition patterns along Ookushi beach in the Goto Island of Japan over a period of 1.5 years. During this time, two webcams installed by the researchers took photographs of the beach every 90 minutes as a means to record high frequency measurements of litter deposition over a large temporal scale. Using these photographs, the researchers approximated the quantity of litter deposited on the beach by using the area of beach covered by litter as a proxy. The results of this study suggested that litter deposition on Ookushi beach fluctuated on a monthly basis and was influenced by wind speed.

3.2 Balloon Photography

Nashima *et al*. (2011) performed a similar study but used data from both in situ measurements and balloon assisted aerial photographs to estimate the amount of MDP deposited on Ookushi beach. This study looked at a single day (October 22, 2009), rather than a period of 1.5 years, and aimed to quantify the amount of debris as well as

to categorize the types of debris. Over 70% of the mass of the items found on the beach via *in situ* measurements was attributed to plastic; however, the researchers concluded that, although this was a cheap and efficient way to measure marine litter deposition on a shoreline, estimates of mass from the aerial photography lacked accuracy.

Kako *et al*. (2012) also used a remote-controlled digital camera held aloft by a helium balloon to capture images of the Seto Inland Sea, Japan. The balloon was kept at a consistent height of approximately 150 m using a line and reel attached to the researcher's boat. To test the accuracy of this remote detection method, the researchers attached GPS tracking devices to 8 differently colored foam rectangular panels and allowed the panels to float freely in the inland sea. The researchers then attempted to identify each of the panels using photographs from the balloon. Although there were distortions in the images due to changes in angle and height of the balloon, the panels' locations were predicted within 1-3 m of their true locations.

3.3 Small Aircraft Photography

In addition to webcams and balloons, airplanes can be a fairly effective method of remotely sensing coastlines to detect MDP. Prichel *et al*. (2012) used images taken from an aircraft to survey targeted locations in the Gulf of Alaska for the GhostNet project, successfully identifying 102 pieces of anthropogenic debris over the period of 14 days. Potential locations for debris accumulation were predicted using satellite data from 6 sources, and these locations were then surveyed.

In 2017, Kataoka, Murray, and Isobe used archived aerial photography to identify macro-litter along the shores of Vancouver Island, Canada. Six thousand, two hundred

and twenty eight aerial photographs taken between October 2014 and March 2015 were ranked on a scale of 0-5, 0 having no visible debris and 5 having significant quantities of evenly distributed debris with multiple varieties visible. A projective transformation was then applied to these images to simulate a directly perpendicular point of observation, and the area of a single pixel calculated, allowing for a relatively accurate estimate of the shoreline surface area covered by MDP. Additionally, the researchers ground-truthed the aerial photography with in-situ site surveys, recording the amount of anthropogenic debris and computing the surface number density using this data as well as the area of the shoreline. This collected information was considered alongside ocean current and wind data from Vancouver Island to assist in determining the cause of site specific densities. It was concluded that specific wind and current condition were favorable for debris accumulation along the shore (Kataoka *et al.,* 2017).

Using 2 DSLR cameras, a medium format aerial camera, and a Cessna 206 airplane, Moy *et al*. (2018) also achieved some success with aircraft-based MDP detection. Over a period of 14 days from August to October 2015, 16 aerial surveys were conducted over the Hawaiian Islands of Niihau, Kauai, Oahu, Molokai, Lanai, Maui, Kahoolawe, and Hawaii, collecting a total of 1223 1.6 km segments of coastline photographic mosaics (Figure 9). By visually examining the segments, the researchers were able to identify and record GPS coordinates for 20,658 individual macro-debris items, ranging from small vessels to buoys to tires. Additionally, “hotspots” where debris had a tendency to accumulate along the windward shores of the islands were identified, allowing organizations interested in removing the debris to focus their efforts on those areas with the highest concentration.

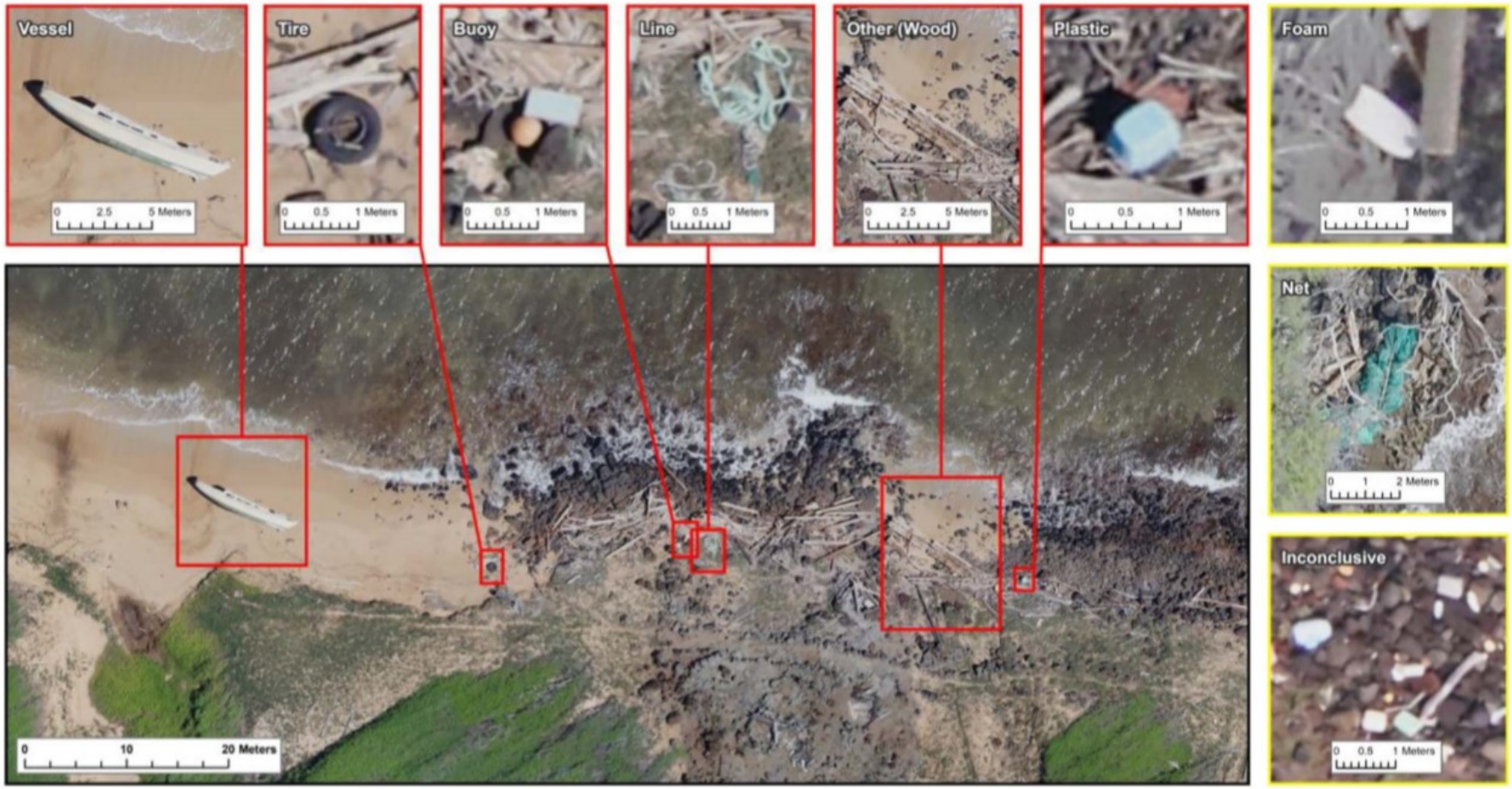

Figure 9. Sample imagery pulled from mosaic image taken from an aircraft over the Hawaiian Islands (Moy et al., 2018). Red boxes indicate items identified as debris in this image. Yellow boxes exhibit other types of debris not included in this particular image.

Despite the success of the study, this method has its weaknesses; the resolution from the aircraft cameras was unable to capture images that would allow the researchers to categorizes items under 0.5 m in diameter, and the area covered per photo was restricted by the 122 meter maximum altitude at which the aircraft was permitted to fly.

3.4 VIS Satellite Imagery

Owing to the high spatial and temporal resolution that is required to remotely sense plastics from satellites in the VIS spectrum, few studies have had success identifying MDP in this manner (National Oceanic and Atmospheric Administration Marine Debris Program, 2015). Whereas some satellites have the ability to deliver over 1 m resolution, this data is normally expensive and often lacking in temporal resolution. Satellites that are capable of collecting images at a high temporal frequency normally have geostationary orbits at altitudes greater than 35,000 km and lack the spatial resolution to be useful for identifying MDP (Mace, 2012).

4. Multispectral Remote Sensing of Marine Debris

Although the above studies have found some success in accounting for MDP using VIS, methods employing the 390-700 nm wavelength range are limited by the spatial and temporal resolutions that are available and by the lack of a distinct signature by which plastic pollution can be identified against dynamic surroundings such as sand and sea foam (Veenstra & Churnside, 2012). However, plastic does have a unique hyperspectral signature that can be utilized to identify plastic remotely.

4.1 Terrestrial Remote Sensing of Plastics

Multispectral remote sensing of plastics was initially utilized in a terrestrial setting. In 2007, Heiden *et al*. used hyperspectral data from the HyMap satellite to construct a spectral library of urban land cover. The authors of this study examined absorption bands, reflectance peaks, increase/decrease of reflectance, brightness, and continuity of a spectral curve to characterize 32 different classes of land cover, 2 of which were polyvinyl chloride and polyethylene. The imagery from the HyMap satellite included 128 bands with 96 bands being in the NIR-SWIR domain. Using these

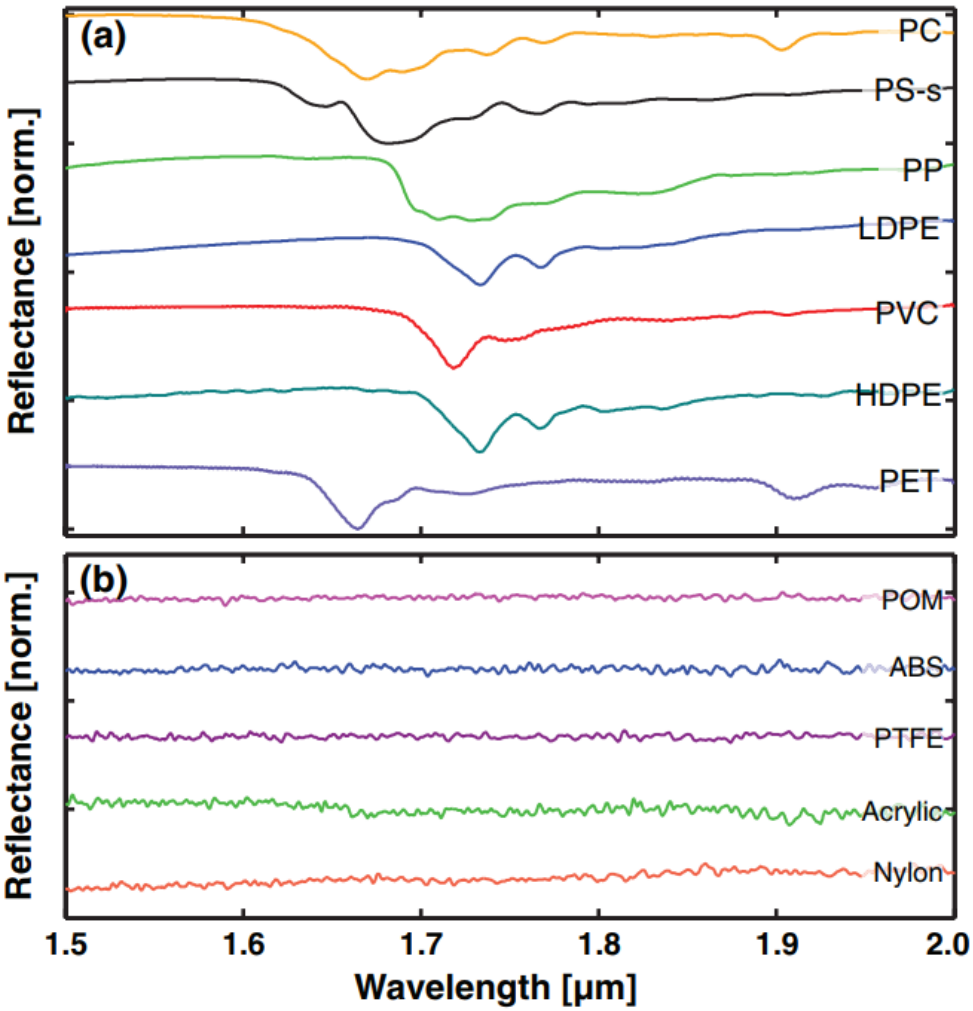

Figure 10. Normalized reflectance spectra of 12 plastic materials (Vázquez-Guardado et al., 2015)

hyperspectral features, Heiden *et al*. achieved commission and omission errors of less than 1% during field tests.

Vázquez-Guardado *et al*. (2015) applied the use of multispectral remotes sensing to identify plastics in municipal waste as a means to recover and separate recyclable plastics. The authors established a library of spectral signatures for 12 plastic resins (Figure 10) and used absorption features in the near infrared (NIR, 1500-2000 nm) and mid-wavelength infrared (MIR, 3000-12000 nm) domains to identify plastic debris in a series of blind detection experiments. Vázquez-Guardado *et al*. discovered that in the NIR domain, there was significant spectral variation in plastics of the same material but different color; this suggested that NIR alone was unable to identify plastics by chemical composition. However, when combined with the MIR spectrum (between 3.0 and 12.0 μm), 22 out of 25 plastic samples were identified confidently as the correct plastic. Of the 25 samples, the only object not identified correctly was a power cord; the authors suggested that fillers in the polymer matrix or the object may have masked its spectral signature.

4.2 Multispectral Remote Sensing in a Marine Environment

When considering the possibility of using multispectral remote sensing data to identify MDP, one must consider the challenges associated with detecting these objects. As plastics tend to change position in suspension with biofouling, these objects are not always directly on the surface of the ocean, and the total exposed area of these plastics changes with the accumulation of colonies of algae and bacteria (Ye & Andrady, 1991). Additionally, the marine “garbage patches” that are referenced by reports and articles are not necessarily large islands of plastic but are instead simply

sections of the ocean that have higher concentrations of plastic pollution. At one time it was believed that these plastic patches mostly consisted of micro-plastics (Moore *et al.,* 2001), which are difficult to detect in the field; however, Lebreton *et al*. (2018) published a study finding that approximately 8% of the plastics recovered from the marine garbage patches were micro-plastics, while the rest were larger. This discovery offers some promise in the struggle for ocean plastic removal, as larger pieces are easier to detect and remove.

As a general rule, the spatial resolution of the sensors used to detect ocean areas with a higher plastic density decreases with distance from the ocean surface (Campbell & Wynne, 2011); depending on the sensor used, only larger pieces of plastic would be possible to sense directly. However, with methods of sub-pixel detection, it is possible to calculate percentages of cover in pixels that contain multiple objects (Yang, *et al.,* 2003).

4.3 Modeling Plastic Reflectance

Goddjin-Murphy *el al.* (2018) proposed that, using sub-pixel detection methods, floating marine plastics could be identified by reflectance despite being smaller in area than the spatial resolution of the sensor. The proposed model suggests considering the reflectance properties of open ocean water as well as reflectance properties of floating plastics in both the VIS and short-wave infrared (SWIR) domains to determine the fractional coverage of ocean surface by plastic. This approximation (Equation 1 and Table 4) makes several assumptions that the authors address.

- The model only considers one type of plastic and assumes 2-dimensionality of the plastic. Marine litter can consist of many different plastic compositions

$$f(\lambda) = \frac{R_t(\lambda) - R_{w,0}(\lambda)}{\rho_{p,RS}(\lambda) + \tau_p(\lambda)1.84(R_{w,0}(\lambda) - \rho_{w,RS}) - R_{w,0}(\lambda)}$$

Equation 1. Equation for determining fractional plastic coverage per pixel (Goddijn-Murphy et al., 2018).

Table 4. List of variables for Equation 1, used to compute fraction of plastic surface coverage (Goddijn-Murphy et al., 2018).

Variable	Definition	Unit
A_p	Area covered by plastic, projected in nadir view	$[m^2]$
A_w	Total area projected in nadir view	$[m^2]$
ε	$L_{ds}/L_{ds,0}$	
f	Plastic area fraction A_p/A_t	
F	Fraction diffuse sky light $E_{d,dif}/E_d$	
E_d	Downwelling irradiance in air	$[wm^{-2}]$
E_{ws}	Upwelling irradiance in water	$[wm^{-2}]$
λ	Wavelength of light	[nm]
L_d	Downwelling radiance in air	$[wm^{-2}sr^{-1}]$
L_{ds}	Downwelling radiance in water	$[wm^{-2}sr^{-1}]$
L_p	Total plastic leaving radiance in air ($L_{pr} + L_{pt}$)[a]	$[wm^{-2}sr^{-1}]$
L_{pr}	L_d reflected by plastic in air[a]	$[wm^{-2}sr^{-1}]$
L_{ps}	Total plastic leaving, downwelling radiance in water	$[wm^{-2}sr^{-1}]$
L_{pt}	L_{ws} transmitted upwards through plastic in air[a]	$[wm^{-2}sr^{-1}]$
L_w	Total water leaving radiance in air ($L_{wr} + L_{wt}$)[a]	$[wm^{-2}sr^{-1}]$
L_{wr}	L_d reflected by air-water interface[a]	$[wm^{-2}sr^{-1}]$
L_{ws}	Sub surface upwelling radiance in water[a]	$[wm^{-2}sr^{-1}]$
L_{wt}	L_{ws} transmitted through water-air interface[a]	$[wm^{-2}sr^{-1}]$
L_t	Total upwelling radiance ($L_w + L_p$)[a]	$[wm^{-2}sr^{-1}]$
R	Ratio of upwelling radiance in nadir view and E_d in air	$[sr^{-1}]$
R_p	L_p/E_d	$[sr^{-1}]$
R_t	L_t/E_d	$[sr^{-1}]$
R_w	L_w/E_d	$[sr^{-1}]$
ρ_p	L_{pr}/L_d	
$\rho_{p,RS}$	L_{pr}/E_d	$[sr^{-1}]$
ρ_{pw}	Fraction of L_{ws} reflected by plastic	
ρ_w	L_{wr}/L_d	
$\rho_{w,RS}$	L_{wr}/E_d	$[sr^{-1}]$
r_{ws}	L_{ws}/L_{ds}	
τ_p	L_{pt}/L_{ws}	
τ_{pw}	Fraction of L_d transmitted through plastic	
τ_w	$L_{ds,0}/L_d$	

and shapes, as well as materials that are not plastic, such as wood and rubber. These variances would likely scatter light differently.

- The model does not account for other plastics interacting with one another to change the behavior of light at the ocean surface. Again, not accounting for the 3-dimensionality of these objects could hinder detection.
- The model considers the surfaces of the plastics to be dry. In reality, the surfaces of the plastics would be wet, and water could fill in cracks at the surface of the plastic object and smooth the signal. This plus the absorption of water in the SWIR region could dull the reflectance of these plastic objects and lead to omission error.

In addition to addressing these assumptions, the authors recommended that, if this approximation were to be used on satellite imagery, specific atmospheric correction algorithms would be required to prevent the concealment of the NIR and SWIR signals identifying the marine litter. Low wind speed conditions would be preferable, as white-capping of the ocean surface could reflect similarly to marine plastics and cause misidentification.

4.4 Laboratory Based Hyperspectral Sensing

Serranti *et al*. (2018) used remote sensing at a very basic level in a study that characterized marine litter collected via trawling nets in the Arctic Sea, the Mediterranean Sea, the South Atlantic Ocean, and North Pacific Ocean. A total of 738 plastic fragments of varying size were collected from 7 sites. Litter was grouped by site and analyzed using a hyperspectral imaging system utilizing the SWIR region.

Spectral data of each plastic fragment were collected and compared with reference spectra. The authors pre-processed the spectral data using 2nd Derivative,

Table 5. Confusion matrix showing actual class vs. predicted class in terms of pixel percentage classified as polyethylene (PE), polypropylene (PP), and polystyrene (PS) (Serranti et al., 2018).

		Actual classes		
		PE	PP	PS
Predicted as	PE	**99.68**	2.17	10.69
Predicted as	PP	0.28	**97.68**	8.01
Predicted as	PS	0.04	0.15	**81.30**

Standard Normal Variate, and Mean Center algorithms; Following this, a principal Component Analysis was applied, finding that two principal components together explained approximately 74% of the variance in data (PC1 = 50.60% and PC2 = 23.48%). This information used to build a classification model, which was applied to hyperspectral images of the plastic litter groups from each site.

This model successfully classified at least 80% of the polymers correctly (Table 5). Although this method would be difficult to apply in the field, in the laboratory it proved to be an efficient and cost-effective analysis of MDP.

4.5 Vibrational Microspectroscopy

Other techniques of analyzing MDP within a laboratory setting, Fourier-transform infrared spectroscopy (FTIR) and Raman Spectroscopy are methods remote sensing that should be noted for their application to nano-plastics (Schymanski *et al.,* 2018). Using these vibrational microspectroscopy techniques, researchers are able to measure plastic particles < 400 µm. Kappler *et al*. (2016) examined both methods as means to detect seawater-suspended micro-plastics that would be otherwise too small for instruments to detect.

Table 6. Comparison between Raman imaging and FTIR transmission imaging when used to detect marine micro-plastics (Kappler et al., 2016).

Raman imaging	FTIR transmission imaging
Number and type of identified microplastics	
• Very small particles (down to 1 μm) can be identified, therefore higher number of detectable microplastics compared to FTIR imaging	• Very small particles (<10 μm) are not detectable (diffraction limit); underestimation of small microplastics (<20 μm)
• Aliphatic and aromatic compounds, C=C compounds are well detectable	• Aliphatic compounds and polyesters are well detectable
• Polyesters (except PET) are difficult to identify correctly	• PVC is difficult to identify correctly
Spectra quality	
• Depends on sample purity	• Depends on sample purity
• Strongly depends on measurement parameters	• Depends on particle size and thickness
• Partially fluorescent	• Thick particles (>50–100 μm) lead to total absorption
Measurement time	
• Long measurement time	• Short measurement time
• Measurement time can be reduced, accompanied by loss of spectra quality and decreasing number of detectable microplastics	• Even large sample areas (up to 10 × 10 mm) can be investigated
Others	
• Problem: focusing of different sized particles (remedy—topographic imaging is possible, but does not work for small transparent particles)	• Created dataset too large for downstream analyses, solely subset can be read out

When using FTIR, MIR radiation is applied to a sample and the transmission and absorption of the sample is measured. These measurements are molecularly specific and rely on changes of the permanent dipole movement of a chemical bond, allowing for the detection of carbonyl groups.

By measuring energy shifts in scattered photons from a laser that is directed on a sample, Raman spectroscopy can also provide information about the molecules in a sample. As opposed to FTIR, Raman spectroscopy utilizes changes in the polarizability of a chemical bond.

Kappler *et al*. (2016) found that although both methods were capable of detecting micro-plastics, the methods complemented each other; some types of plastics were more easily detected by Raman spectroscopy, others were more readily identified by FTIR (Table 6). Raman spectroscopy was able to identify other characteristics about the particles, such as fillers and pigments that FTIR missed; however, Raman spectroscopy misidentified some particles that FTIR correctly identified. Overall, Raman spectroscopy could detect smaller sized plastic particles, but also took significantly more time.

4.6 Aerial and Satellite Multispectral Detection

Despite continually improving technology and understanding of MDP transport and behavior, there still has been little success using multispectral remote sensing to identify MDP via aircraft or satellite (Veenstra & Churnside, 2012). However, there have been some spectral imaging studies that have explored this field and returned some promising results.

A study conducted by Garaba and Dierssen (2018) tested satellite multispectral remote sensing as a means of detecting plastic debris using absorption features at 1215

and 1732 nm. In order to establish a spectral library for plastic resins, the authors used a PANalytical Boulder ASD FieldSpec 4 spectroradiometer to measure the spectral signature of 11 plastic resin pellets:

- polyvinyl chloride
- polyamide
- nylon
- low-density polyethylene
- polyethylene terephthalate
- polypropylene (PP)
- fluorinated ethylene propylene teflon
- terpolymer lustran 752
- polystyrene
- fluorinated polymethyl methacrylate
- Merlon.

In addition to these materials, the authors measured the spectral reflectance of a large collection dry marine-harvested macro-plastics that had experienced weathering so as to build a spectral library representative of what might be found in the field (Garaba & Dierssen, 2018).

Following this, spectra was measured of samples of plastics, both dry and floating in filtered seawater. These spectra were averaged and processed to quantify major absorption features in both dry and wet plastics. These common absorption features (Figure 11) were identified as:

- 905 – 955 nm
- 1160 – 1260 nm
- 1380 – 1480 nm
- 1715 – 1750 nm

When increased pixel coverage was simulated (constructing a scenario where a pixel encompasses the plastic as well as sea water), both dry and wet plastics exhibited reductions in the depth of the 1215 nm and 1732 nm absorption features. The absorption feature depth of wet plastics, however, decreased 3 times as much as dry plastics in the 1215 nm band and 5 times as much in the 1732 band when compared with dry plastics, due to water masking the indicative plastic spectral features (Figure 12). This result of spectral mixing proved to be a hurdle when applied in this feasibility study.

Testing this analysis, an assessment of hyperspectral remotely sensed plastic detection was conducted over the Sunshine Canyon Landfill in California, USA using aerial imagery with a spatial resolution of 7.1 m collected from the Airborne Visible/Infrared Imaging Spectrometer (AVIRIS), a multispectral airborne sensor with a spectral resolution of 224 bands (Figure 13). Of the common absorption features characterized in the spectral analysis, two coincided with absorption features of water vapor (~950 nm and ~1400 nm); thus, bands with a center wavelength of 1215 nm and 1732 nm were examined. Using these bands and previous analyses, a hydrocarbon index was created for the purpose of mapping materials with hydrocarbon components, such as plastics.

Terrestrial features such as plastic rooftops and the landfill were detectable using the hydrocarbon index and AVIRIS imagery. There was an overlap in absorption features of vegetation and plastics, but the authors suggested that a normalized difference vegetation index could be used to separate these vegetation pixels from those identifying plastics. Detecting plastic debris in water proved to be more difficult; while the authors stated there are common NIR/SWIR absorption features that exist in hydrocarbons, a high concentration of buoyant particles and a satellite with a high spatial resolution would be required to make clear identifications.

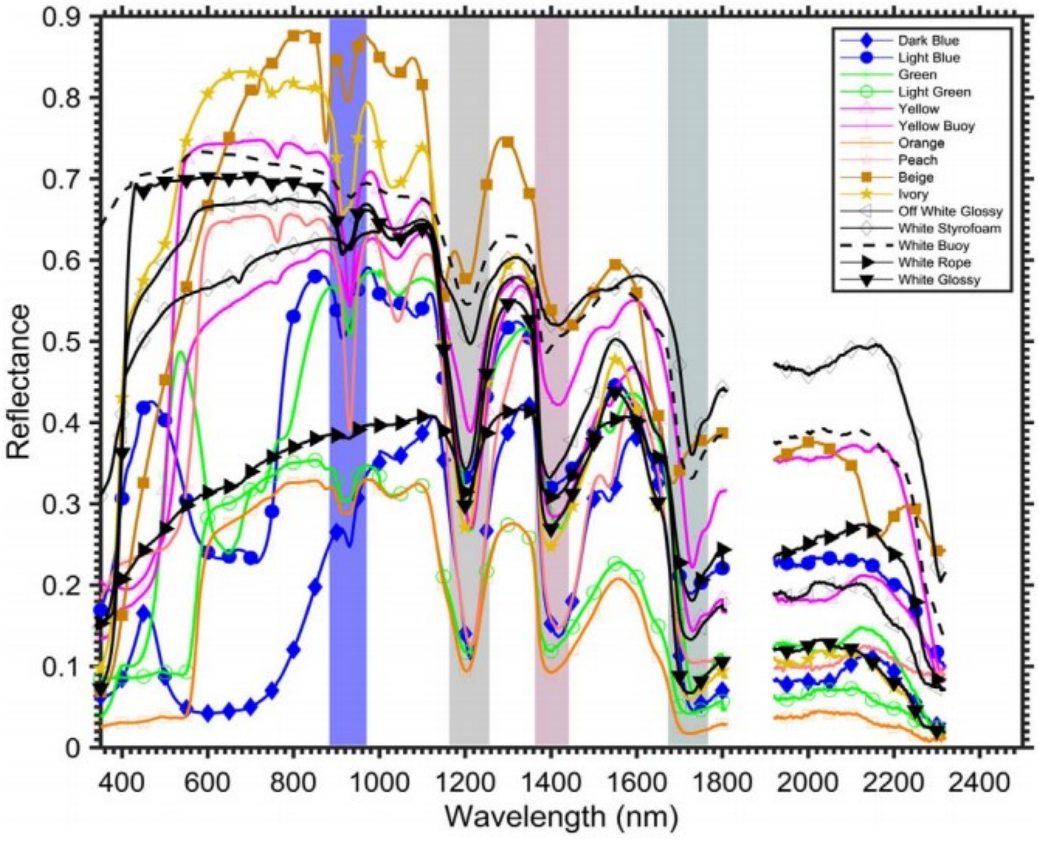

Figure 11. Reflectance spectra of unknown marine-harvested plastics. Shaded regions indicate common absorption features (Garaba & Dierssen, 2018).

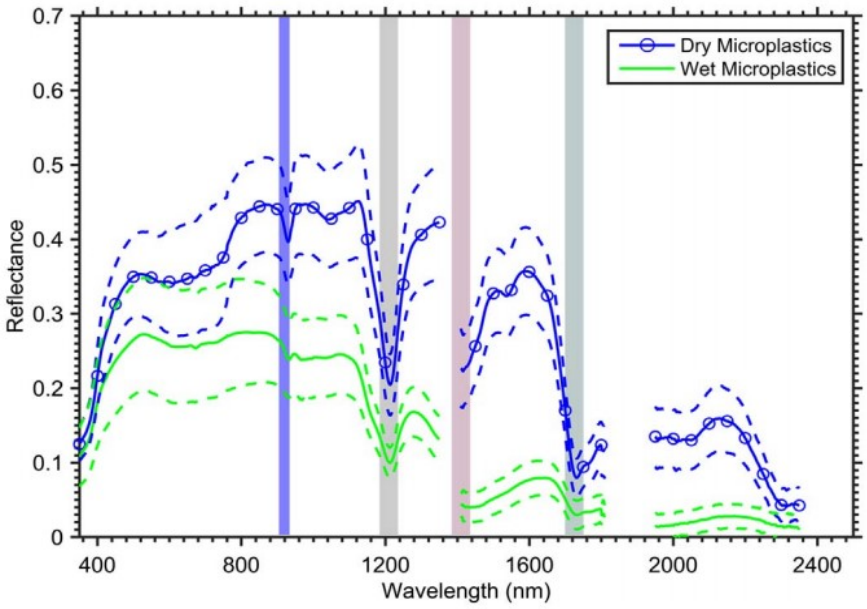

Figure 12. Comparison of reflectance spectra of wet and dry micro-plastics. Shaded regions indicate common spectral absorption features (Garaba & Dierssen, 2018).

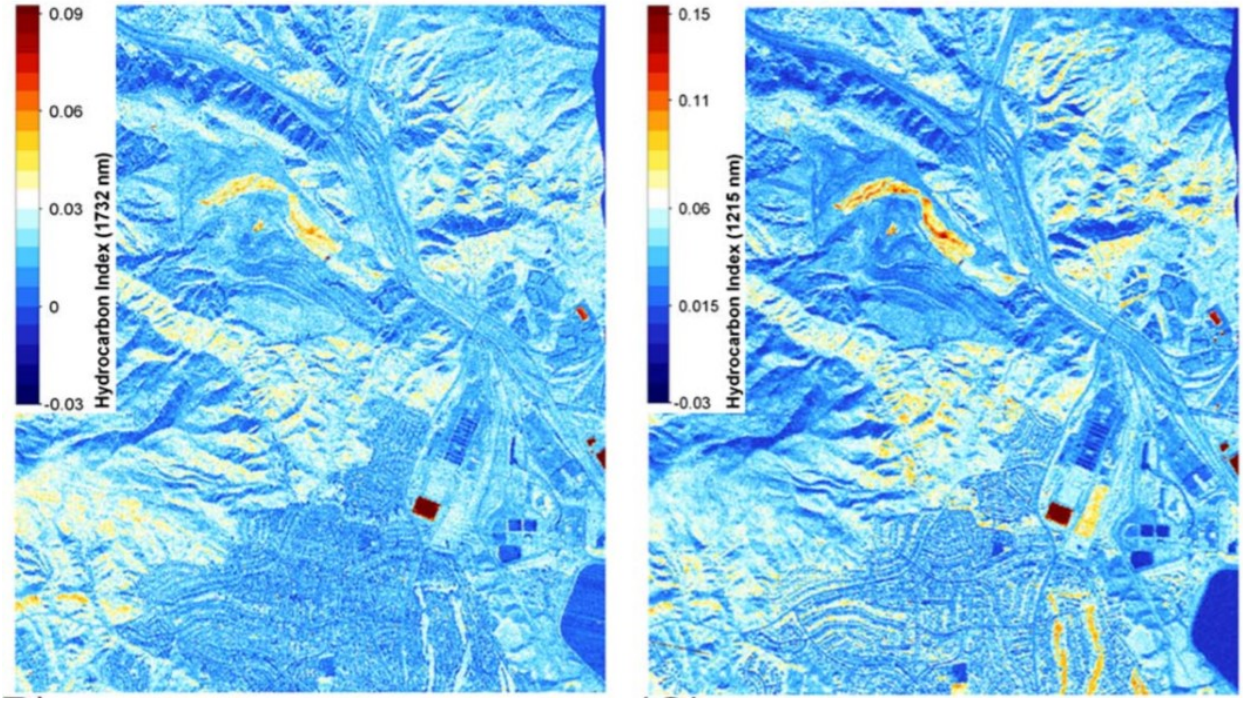

Figure 13. Hydrocarbon index map of Sunshine Canyon Landfill (Garaba & Dierssen, 2018). Left image shows the index for absorption feature at 1732, right image shows index for absorption feature 1215 nm. Higher index value indicates higher likelihood of hydrocarbon material.

Although the spatial and temporal resolution of multispectral data is a significant obstacle to overcome when detecting MDP via satellite, there have been significant improvements in satellite sensors that may allow for this possibility to become a reality. WorldView-3, a multispectral satellite launched in 2014, could have the potential to detect plastic debris from space. Asadzadeh and de Souza Filho (2016) tested the capabilities of the WorldView-3 satellite in detecting hydrocarbons in the form of oil in sediments by first collecting airborne and close range hyperspectral data using a ProSpecTIR airborne imager and a sisuChema imaging system, and then resampling this data to the 7.5 m spatial resolution and the 28 band spectral resolution of WorldView-3. The results of this study indicated that WorldView-3 was suitable for detecting hydrocarbons, but the authors suggested that more research needed to be conducted in order to determine if this would work in a marine environment.

5. SAR Detection of Marine Debris

Some studies have found success using wavelengths longer than 1 cm to remotely detect MDP. These longer wavelengths have the ability to penetrate cloud cover, making this domain of EMR useful during overcast weather conditions which would normally obscure remotely sensed observations (Koyama *et al*., 2016). Synthetic aperture radar (SAR), which involves sending multiple long wave EMR pulses from a

Table 7. Specifications of SAR sensors used to identify tsunami debris (Arii, Koiwa, & Aoki, 2014).

Sensor	PALSAR	CSK	RS2
Band	L	X	C
Wavelength (cm)	24	3	6
Range resolution (m)	10	5	15
Azimuth resolution (m)	5	5	8
Pixel spacing (m)	6.25	2.5	6.25
Swath (km)	60	40	170

sensor towards the ocean surface and recording the resulting reflection, has been used to identify macro-debris clusters on the ocean surface. As with many of the preceding methods, this method is best used to detect superficial debris, as the longwave EMR pulses cannot penetrate the ocean surface.

The infamous 2011 Tohoku tsunami, albeit a tragedy, was a stage for researchers to test means to detect and track MDP from a catastrophic incident (NOAA, 2015). Arii *et al.* (2014) chose to examine the feasibility of SAR to detect debris from the catastrophic event. Using 3 separate SAR sensors (Table 7), the authors set out to identify macro-debris position and size as well as to estimate the movement of the debris (Figure 14).

After identifying several MDP clusters and estimating their surface coverage through SAR, Arii *et al.* established a series of stages with plans for optimum post-tsunami debris monitoring with SAR.

- Stage 1: Encompassing the first 24 hours following the catastrophe, Stage I should include frequent observations with a wide swath width at medium resolution. This is deemed most effective when considering the importance of identifying initial locations and trajectories of plastics before debris disperses.
- Stage 2: In the next 24 hours following Stage I, swath width should be narrowed and resolution increased. Additionally, multiple polarizations and incident angles every couple of hours should be routine. During Stage II, water that flowed over the coastal plains has started to return to the ocean; tracking MDP and ocean currents is important both in following MDP paths as

well is aiding in search and rescue operations, and higher resolution imagery offers better detail in these regards.

- Stage 3: The final stage of monitoring can be accomplished primarily with satellite-based imagery and particle tracking models alongside model verification by SAR sensors. The authors proposed an equation to determine appropriate swath width (Equation 2), where V_{max} represents the maximum velocity models by particle tracking simulations, X represents swath width, and T is the time interval.

$$V_{\max} = \frac{X}{T}$$

Equation 2. Equation determining recommended SAR swath width (X), using maximum observed velocity of debris Vmax and time interval (T) (Arii et al., 2014).

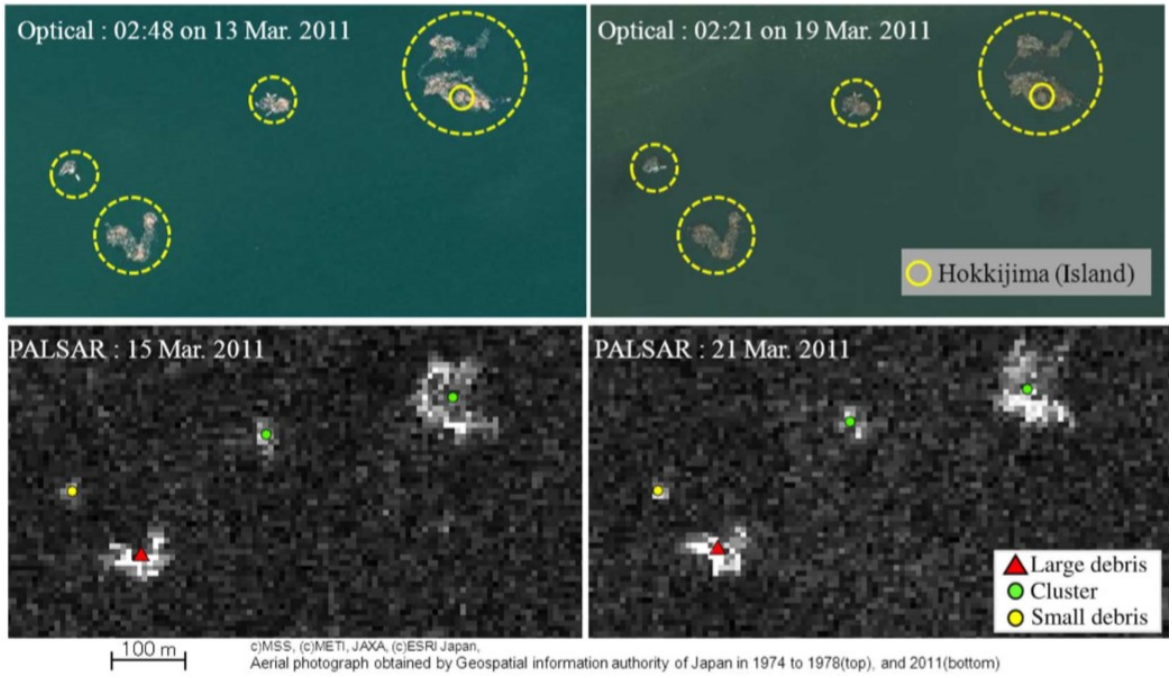

Figure 14. Aerial photos (top) of tsunami debris and PALSAR images (bottom) taken on March 13th (left) and March 19th, 2011 (Arii et al., 2014). Colored shapes denote classification of debris.

6. Application of Marine Debris Detection Data

The previous sections illustrated the capabilities of remote sensing to provide data on the locations and movements of MDP. Understanding the behavior of plastic pollutants in our oceans is crucial to understanding how best to remedy this environmental predicament. Although there is no simple solution to this problem, there have been many attempts made to address both the effects and sources of MDPP, ranging from policy measures to on-the-ground clean-up efforts.

NOAA's Marine Debris Program has been a major player in facilitating organized marine litter clean-ups and in educating the public about MDP (NOAA, 2017). In 2017 alone, this program removed 1,600 MT of debris from shorelines and waterways. In addition to cleanups, NOAA has also funded the installation of infrastructure designed to limit debris influx from inland waterways. For example, NOAA provided funding to the County of Prince George for the establishment of two floating litter traps designed to catch floating debris in the Anacostia River before it flows to the Chesapeake Bay. Projects like these could certainly benefit from remotely sensed data identifying point sources of MDP and the movement of MDP into marine waterways.

The Ocean Cleanup organization is also attempting to undertake a large-scale ocean clean-up project, but rather than relying on manpower, the non-profit plans to utilize passive drifting debris collectors to consolidate MDP for removal (Figure 15). In the organization's feasibility study (Slat, 2014), several important facets of this project were explored, including environmental impacts, durability of the collectors, and viability of the project. Slat calculated that the device could potentially collect 79% of the plastics encountered and could do so with limited environmental impact. Rochman (2016)

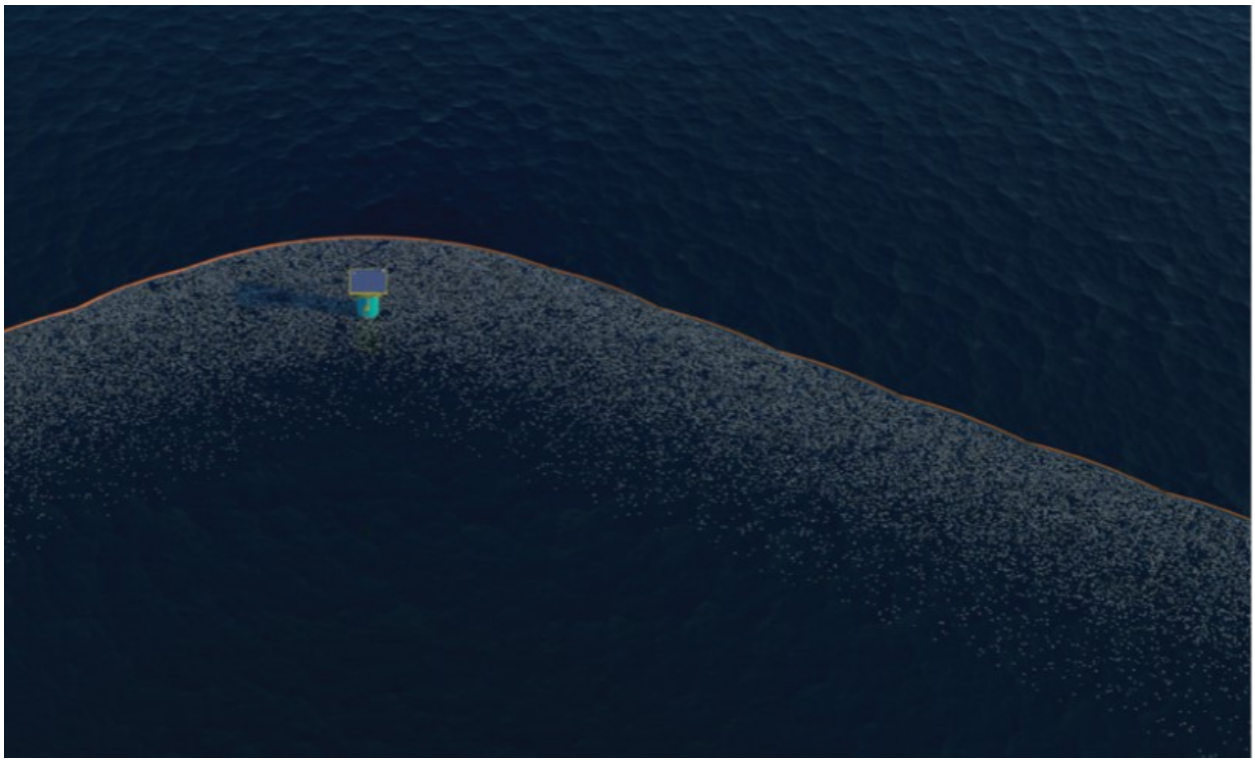

Figure 15. Proposed Ocean Cleanup Passive Collector (Slat, 2014). Image shows orange extended barriers funneling plastics towards the collection platform.

suggested that placement of these devices would be key to the success of the project, even going so far as to say that installing passive debris catchers in the ocean gyres as recommended by Slat would be unwise, and that installation nearer to the coast would be better suited to catch debris before it sinks or is consumed by marine animals. The deployment of this technology could be greatly enhanced by remotely sensed data of MDP; understanding the movement and collection of debris in ocean environments will certainly help guide the Ocean Cleanup team in consideration of placement of this technology and could potentially assist in assessing the effectiveness of the program.

Legislation regarding the manufacturing and disposal of plastics enacted in parallel with cleanup efforts will be crucial to remediation of ocean plastic pollution. As an example, the Microbead Free Waters Act of 2015 helped to put an end to the use of

plastic microbeads in cosmetics, severely diminishing what was once a huge source of micro-plastic pollution (McDevitt *et al.,* 2017). Policies such as the Microbead Free Waters Act and California SB 270, which put a tax on plastic shopping bags and eliminated the sale of these bags in the State of California, are the backbone of the fight against MDP; by cutting off sources of plastic pollution, a once impossible task of ridding marine ecosystems of plastic becomes plausible. Using remote sensing to aid in systems to collect MDP data could influence and inspire more plastic controlling legislation, an invaluable service in the fight against this problem.

7. Conclusion

It is clear that there are benefits to using remote sensing as a means to provide information about MDP concentrations and trajectories. When using models, remotely sensed data can provide observations on a global scale that can help to improve model outputs, aiding in the prediction of the path and velocity of MDP. In some cases, debris is directly sensible, allowing researchers to estimate amounts of debris and identify points of accumulation along shorelines. Satellite and aerial images have been used to identify clusters of MDP for removal, and post-disaster SAR measurements have allowed researchers to track debris movement. These methods, however, are only as good as the technology that supports them. The lack of resolution, whether it be temporal, spatial, or spectral, is currently a crux in the mission to detect, remove, and prevent MDP pollution. Considering the current technology, using models aided by remotely sensed data to locate probable areas of MDP accumulation and subsequently collecting high spatial resolution observations of these targeted locations using aerial or satellite sensors would be the most effective method of identifying and quantifying MDP.

Improvement of satellite and aerial sensors will greatly enhance these methods and potentially allow for accurate data that can be used to plan mitigation efforts and design effective plastic legislation.

8. References

Andrady, A. L. (Ed.). (2003). Plastics and the environment. Hoboken, N.J: Wiley-Interscience.

Andrady, A. L., & Neal, M. A. (2009). Applications and societal benefits of plastics. Philosophical Transactions of the Royal Society B: Biological Sciences, 364(1526), 1977–1984. https://doi.org/10.1098/rstb.2008.0304

Andrady, Anthony L. (2011). Microplastics in the marine environment. Marine Pollution Bulletin, 62(8), 1596–1605. https://doi.org/10.1016/j.marpolbul.2011.05.030

Arii, M., Koiwa, M., & Aoki, Y. (2014). Applicability of SAR to Marine Debris Surveillance After the Great East Japan Earthquake. IEEE Journal of Selected Topics in Applied Earth Observations and Remote Sensing, 7(5), 1729–1744. https://doi.org/10.1109/JSTARS.2014.2308550

Asadzadeh, S., & de Souza Filho, C. R. (2016). Investigating the capability of WorldView-3 superspectral data for direct hydrocarbon detection. Remote Sensing of Environment, 173, 162–173. https://doi.org/10.1016/j.rse.2015.11.030

Auta, H. S., Emenike, C., & Fauziah, S. . (2017). Distribution and importance of microplastics in the marine environment: A review of the sources, fate, effects, and potential solutions. Environment International, 102, 165–176. https://doi.org/10.1016/j.envint.2017.02.013

Barnes, D. K. A., Galgani, F., Thompson, R. C., & Barlaz, M. (2009). Accumulation and fragmentation of plastic debris in global environments. Philosophical Transactions of the Royal Society B: Biological Sciences, 364(1526), 1985–1998. https://doi.org/10.1098/rstb.2008.0205

Bonjean, F., & Lagerloef, G. S. E. (2002). Diagnostic Model and Analysis of the Surface Currents in the Tropical Pacific Ocean. Journal of Physical Oceanography, 32(10), 2938–2954. https://doi.org/10.1175/1520-0485(2002)032<2938:DMAAOT>2.0.CO;2

Campbell, J. B., & Wynne, R. H. (2011). Introduction to Remote Sensing (5th ed.). Guiliford Press.

Cheung, P. K., & Fok, L. (2017). Characterisation of plastic microbeads in facial scrubs and their estimated emissions in Mainland China. Water Research, 122, 53–61. https://doi.org/10.1016/j.watres.2017.05.053

Cincinelli, A., Scopetani, C., Chelazzi, D., Lombardini, E., Martellini, T., Katsoyiannis, A., … Corsolini, S. (2017). Microplastic in the surface waters of the Ross Sea (Antarctica): Occurrence, distribution and characterization by FTIR. Chemosphere, 175,

391–400. https://doi.org/10.1016/j.chemosphere.2017.02.024

Cooper, D. A., & Corcoran, P. L. (2010). Effects of mechanical and chemical processes on the degradation of plastic beach debris on the island of Kauai, Hawaii. Marine Pollution Bulletin, 60(5), 650–654. https://doi.org/10.1016/j.marpolbul.2009.12.026

Dohan, K., & Maximenko, N. (2010). Monitoring Ocean Currents with Satellite Sensors. Oceanography, 23(4), 94–103. https://doi.org/10.5670/oceanog.2010.08

Duhec, A. V., Jeanne, R. F., Maximenko, N., & Hafner, J. (2015). Composition and potential origin of marine debris stranded in the Western Indian Ocean on remote Alphonse Island, Seychelles. Marine Pollution Bulletin, 96(1–2), 76–86. https://doi.org/10.1016/j.marpolbul.2015.05.042

Earth and Space Research. (2009). OSCAR third degree resolution ocean surface currents. Retrieved March 24, 2018, from https://podaac.jpl.nasa.gov/dataset/OSCAR_L4_OC_third-deg

Garaba, S. P., & Dierssen, H. M. (2018). An airborne remote sensing case study of synthetic hydrocarbon detection using short wave infrared absorption features identified from marine-harvested macro- and microplastics. Remote Sensing of Environment, 205, 224–235. https://doi.org/10.1016/j.rse.2017.11.023

Geyer, R., Jambeck, J. R., & Law, K. L. (2017). Production, use, and fate of all plastics ever made. Science Advances, 3(7), e1700782.

Gloag, J. (1943). The Influence of Plastics on Design. Journal of the Royal Society of Arts, 91(4644), 461–470.

Goddijn-Murphy, L., Peters, S., van Sebille, E., James, N. A., & Gibb, S. (2018). Concept for a hyperspectral remote sensing algorithm for floating marine macro plastics. Marine Pollution Bulletin, 126, 255–262. https://doi.org/10.1016/j.marpolbul.2017.11.011

Heiden, U., Segl, K., Roessner, S., & Kaufmann, H. (2007). Determination of robust spectral features for identification of urban surface materials in hyperspectral remote sensing data. Remote Sensing of Environment, 111(4), 537–552. https://doi.org/10.1016/j.rse.2007.04.008

Hosler, D. (1999). Prehistoric Polymers: Rubber Processing in Ancient Mesoamerica. Science, 284(5422), 1988–1991. https://doi.org/10.1126/science.284.5422.1988

Hong, S., & Shin, I. (2013). Wind Speed Retrieval Based on Sea Surface Roughness Measurements from Spaceborne Microwave Radiometers. Journal of Applied Meteorology and Climatology, 52(2), 507–516. https://doi.org/10.1175/JAMC-D-11-0209.1

Jambeck, J. R., Geyer, R., Wilcox, C., Siegler, T. R., Perryman, M., Andrady, A., Lavender Law, K. (2015). Plastic waste inputs from land into the ocean. Science, 347(6223), 768–771. https://doi.org/10.1126/science.1260352

Jet Propulsion Laboratory, C. I. of T. (n.d.). Technology. Retrieved March 24, 2018, from https://sealevel.jpl.nasa.gov/technology/

Kako, S., Isobe, A., & Magome, S. (2010). Sequential monitoring of beach litter using webcams. Marine Pollution Bulletin, 60(5), 775–779. https://doi.org/10.1016/j.marpolbul.2010.03.009

Kako, S., Isobe, A., & Magome, S. (2012). Low altitude remote-sensing method to monitor marine and beach litter of various colors using a balloon equipped with a digital camera. Marine Pollution Bulletin, 64(6), 1156–1162. https://doi.org/10.1016/j.marpolbul.2012.03.024

Käppler, A., Fischer, D., Oberbeckmann, S., Schernewski, G., Labrenz, M., Eichhorn, K.-J., & Voit, B. (2016). Analysis of environmental microplastics by vibrational microspectroscopy: FTIR, Raman or both? Analytical and Bioanalytical Chemistry, 408(29), 8377–8391. https://doi.org/10.1007/s00216-016-9956-3

Kataoka, T., Murray, C. C., & Isobe, A. (2017). Quantification of marine macro-debris abundance around Vancouver Island, Canada, based on archived aerial photographs processed by projective transformation. Marine Pollution Bulletin. https://doi.org/10.1016/j.marpolbul.2017.08.060

Koyama, C. N., Gokon, H., Jimbo, M., Koshimura, S., & Sato, M. (2016). Disaster debris estimation using high-resolution polarimetric stereo-SAR. ISPRS Journal of Photogrammetry and Remote Sensing, 120, 84–98. https://doi.org/10.1016/j.isprsjprs.2016.08.003

Kubota, M. (1994). A Mechanism for the Accumulation of Floating Marine Debris North of Hawaii. Journal of Physical Oceanography, 24, 1059–1064.

Kühn, F., Oppermann, K., & Hörig, B. (2004). Hydrocarbon Index – an algorithm for hyperspectral detection of hydrocarbons. International Journal of Remote Sensing, 25(12), 2467–2473. https://doi.org/10.1080/01431160310001642287

Lagerloef, G. S. E., Mitchum, G. T., Lukas, R. B., & Niiler, P. P. (1999). Tropical Pacific near-surface currents estimated from altimeter, wind, and drifter data. Journal of Geophysical Research: Oceans, 104(C10), 23313–23326. https://doi.org/10.1029/1999JC900197

Larnicol, G., Guinehut, S., Drévillon, M., Faugere, Y., & Nicolas, G. (2006). The global observed ocean products of the French Mercator project. European Space Agency Special Publication.

Lebreton, L., Slat, B., Ferrari, F., Sainte-Rose, B., Aitken, J., Marthouse, R., Reisser, J. (2018). Evidence that the Great Pacific Garbage Patch is rapidly accumulating plastic. Scientific Reports, 8(1). https://doi.org/10.1038/s41598-018-22939-w

Lebreton, L. C.-M., & Borrero, J. C. (2013). Modeling the transport and accumulation floating debris generated by the 11 March 2011 Tohoku tsunami. Marine Pollution Bulletin, 66(1–2), 53–58. https://doi.org/10.1016/j.marpolbul.2012.11.013

Mace, T. H. (2012). At-sea detection of marine debris: Overview of technologies, processes, issues, and options. Marine Pollution Bulletin, 65(1–3), 23–27. https://doi.org/10.1016/j.marpolbul.2011.08.042

Maes, C., & Blanke, B. (2015). Tracking the origins of plastic debris across the Coral Sea: A case study from the Ouvéa Island, New Caledonia. Marine Pollution Bulletin, 97(1–2), 160–168. https://doi.org/10.1016/j.marpolbul.2015.06.022

Mattsson, K., Hansson, L.-A., & Cedervall, T. (2015). Nano-plastics in the aquatic environment. Environmental Science: Processes & Impacts, 17(10), 1712–1721. https://doi.org/10.1039/C5EM00227C

Maximenko, N., Chao, Y., & Moller, D. (2016). Developing a remote sensing system to track marine debris. Eos, 97. https://doi.org/10.1029/2016EO061605

Maximenko, Nikolai, Arvesen, J., Asner, G., Carlton, J., College, W., Castrence, M., Kataoka, T. (2016). Remote sensing of marine debris to study dynamics, balances and trends. Decadal Survey for Earth Science and Applications from Space, 22.

Maximenko, Nikolai, & Hafner, J. (2010). SCUD: surface currents from diagnostic model. IPRC Tech. Note, 5, 17.

McDevitt, J. P., Criddle, C. S., Morse, M., Hale, R. C., Bott, C. B., & Rochman, C. M. (2017). Addressing the Issue of Microplastics in the Wake of the Microbead-Free Waters Act—A New Standard Can Facilitate Improved Policy. Environmental Science & Technology, 51(12), 6611–6617. https://doi.org/10.1021/acs.est.6b05812

McElwee, K., Donohue, M. J., Courtney, C. A., Morishige, C., & Rivera-Vicente, A. (2012). A strategy for detecting derelict fishing gear at sea. Marine Pollution Bulletin, 65(1–3), 7–15. https://doi.org/10.1016/j.marpolbul.2011.09.006

Meeker, J. D., Sathyanarayana, S., & Swan, S. H. (2009). Phthalates and other additives in plastics: human exposure and associated health outcomes. Philosophical Transactions of the Royal Society B: Biological Sciences, 364(1526), 2097–2113. https://doi.org/10.1098/rstb.2008.0268

Moore, C. J., Moore, S. L., Leecaster, M. K., & Weisberg, S. B. (2001). A comparison of plastic and plankton in the North Pacific central gyre. Marine Pollution Bulletin, 42(12), 1297–1300.

Moy, K., Neilson, B., Chung, A., Meadows, A., Castrence, M., Ambagis, S., & Davidson, K. (2017). Mapping coastal marine debris using aerial imagery and spatial analysis. Marine Pollution Bulletin. https://doi.org/10.1016/j.marpolbul.2017.11.045

Nakashima, E., Isobe, A., Magome, S., Kako, S., & Deki, N. (2011). Using aerial photography and in situ measurements to estimate the quantity of macro-litter on beaches. Marine Pollution Bulletin, 62(4), 762–769. https://doi.org/10.1016/j.marpolbul.2011.01.006

National Oceanic and Atmospheric Administration Marine Debris Program. (2014a). Report on the Entanglement of Marine Species in Marine Debris with an Emphasis on Species in the United States (p. 28). Silver Spring, MDP: National Oceanic and Atmospheric Administration Marine Debris Program.

National Oceanic and Atmospheric Administration Marine Debris Program. (2014b). Report on the Occurrence and Health Effects of Anthropogenic Debris Ingested by Marine Organisms (p. 19). Silver Spring, MDP: National Oceanic and Atmospheric Administration Marine Debris Program.
National Oceanic and Atmospheric Administration Marine Debris Program. (2015). Japan Tsunami Marine Debris Detection Report: A Synthesis of Efforts and Lessons Learned (Technical Memorandum No. NOS-OR&R-51). U.S. Department of Commerce.

National Oceanic and Atmospheric Administration Marine Debris Program. (2016a). Report on Marine Debris Impacts on Coastal and Benthic Habitats. Silver Spring, MDP: National Oceanic and Atmospheric Administration Marine Debris Program.

National Oceanic and Atmospheric Administration Marine Debris Program. (2016b). Report on Modeling Oceanic Transport of Floating Marine Debris (p. 21). Silver Spring, MDP: National Oceanic and Atmospheric Administration Marine Debris Program.

National Oceanic and Atmospheric Administration Marine Debris Program. (2017). Report on Marine Debris as a Potential Pathway for Invasive Species. Silver Spring, MDP: National Oceanic and Atmospheric Administration Marine Debris Program.

NOAA Satellite Information System (NOAASIS). (2017, July 10). Retrieved March 24, 2018, from http://noaasis.noaa.gov/NOAASIS/ml/avhrr.html

Physical Oceanography DAAC. (2001). SeaWinds on QuikSCAT Level 3 Daily, Gridded Ocean Wind Vectors (JPL SeaWinds Project) (Guide Document No. 1.1). JPL, California Institute of Technology.

PlasticsEurope. (n.d.). World Plastics Production 1950 -2005 [PowerPoint slides]. Retrieved from https://committee.iso.org/files/live/sites/tc61/files/The%20Plastic%20-Industry%20Berlin-%20Aug%202016%20-%20Copy.pdf

Reisser, J., Slat, B., Noble, K., du Plessis, K., Epp, M., Proietti, M., Pattiaratchi, C. (2015). The vertical distribution of buoyant plastics at sea: an observational study in the North Atlantic Gyre. Biogeosciences, 12(4), 1249–1256. https://doi.org/10.5194/bg-12-1249-2015

Rochman, C. M. (2016). Strategies for reducing ocean plastic debris should be diverse and guided by science. Environmental Research Letters, 11(4), 041001. https://doi.org/10.1088/1748-9326/11/4/041001

Schymanski, D., Goldbeck, C., Humpf, H.-U., & Fürst, P. (2018). Analysis of microplastics in water by micro-Raman spectroscopy: Release of plastic particles from different packaging into mineral water. Water Research, 129, 154–162. https://doi.org/10.1016/j.watres.2017.11.011

Secretariat of the Convention on Biological Diversity (SCBD) and the Scientific and Technical Advisery Panel-GEF. (2012). Impacts of marine debris on biodiversity: current status and potential solutions. Montreal. Technical Series No. 67. 61 pp.

Serranti, S., Palmieri, R., Bonifazi, G., & Cózar, A. (2018). Characterization of microplastic litter from oceans by an innovative approach based on hyperspectral imaging. Waste Management. https://doi.org/10.1016/j.wasman.2018.03.003

Slat, B. (2014). How the Oceans Can Clean Themselves: A Feasibility Study (No. 2.0). The Ocean Cleanup.

Sudre, J., & Morrow, R. A. (2008). Global surface currents: a high-resolution product for investigating ocean dynamics. Ocean Dynamics, 58(2), 101–118. https://doi.org/10.1007/s10236-008-0134-9

Summers, J. W., & Rabinovitch, E. B. (1999). Weatherability of Vinyl and Other Plastics. In G. Wypych (Ed.), Weathering of Plastics (pp. 61–68). William Andrew Inc.

Jet Propulsion Laboratory. (n.d.). *Technology.* Retrieved from https://sealevel.jpl.nasa.gov/technology/

Thompson, R. C., Moore, C. J., vom Saal, F. S., & Swan, S. H. (2009). Plastics, the environment and human health: current consensus and future trends. Philosophical Transactions of the Royal Society B: Biological Sciences, 364(1526), 2153–2166. https://doi.org/10.1098/rstb.2009.0053

Vázquez-Guardado, A., Money, M., McKinney, N., & Chanda, D. (2015). Multi-spectral infrared spectroscopy for robust plastic identification. Applied Optics, 54(24), 7396.

https://doi.org/10.1364/AO.54.007396

Veenstra, T. S., & Churnside, J. H. (2012). Airborne sensors for detecting large marine debris at sea. Marine Pollution Bulletin, 65(1–3), 63–68. https://doi.org/10.1016/j.marpolbul.2010.11.018

Wiebe, B. E., Hughes, T. P., & Pinch, T. J. (1987). The Social Construction of Technological Systems: New Directions in the Sociology and History of Technology. MIT Press.

Yang, L., Xian, G., Klaver, J. M., & Deal, B. (2003). Urban Land-Cover Change Detection through Sub-Pixel Imperviousness Mapping Using Remotely Sensed Data. Photogrammetric Engineering & Remote Sensing, 69(9), 1003–1010. https://doi.org/10.14358/PERS.69.9.1003

Ye, S., & Andrady, A. L. (1991). Fouling of floating plastic debris under Biscayne Bay exposure conditions. Marine Pollution Bulletin, 22(12), 608–613.